

CFRP STRENGTHENING OF PRE-DAMAGE RC BEAMS.

Brwa HS Hamah-Ali *

* PhD and senior lecturer at civil engineering department, college of engineering, university of Sulaimani.

Brwa.hamahali@univsul.edu.iq

ABSTRACT

In order to investigate the effect of pre-loading damage on the structural performance of CFRP strengthened R.C. beams, experimental and FEM investigation was carried out on six R.C. beams. Five of the R.C. beams were damaged up to different levels of strain in the main steel bars before strengthening. One of the R.C. beams loaded up to failure and was kept as a control beam for comparison. The experimental results showed that the failure mode of the CFRP strengthened specimen was controlled by CFRP debonding followed by concrete crushing; however, the control beam failed in concrete crushing after yielding the steel bars, which is a ductile failure. The CFRP sheet increases the strength and initial stiffness of the R.C. beams and reduces ductility and toughness. Also, CFRP application increases the first crack and yielding steel bars load by 87.4% and 34.4%, respectively. Furthermore, the pre-damage level does not influence the strength and ductility of the strengthened R.C. beams except for the highest damage levels, which experienced a slight decrease in load capacity and ductility. However, the initial stiffness decreases with increasing pre-damage levels by 40%.

ACI 440.2R predicts the ultimate load capacity marvelously for externally bonded FRP beams compared to the experimental ultimate load capacity. The fact that the experiment and the FEM agree so well implies that the concrete and reinforcement constitutive models, as well as the cohesive interface model, may accurately represent failure mode. However, Because of the expected perfect bond between concrete and reinforcement, the FEM analysis indicates that the beam will be slightly stiffer and stronger. The developed FEM can be used for further parametric study.

Keywords: Pre-loading, damaged R.C. beams, CFRP, strengthening, FEM, debonding, toughness, ductility.

Table of Content

INTRODUCTION	3
RESEARCH SIGNIFICANCE.....	8
EXPERIMENTAL WORK.....	8
2.1. CONCRETE MIX PROPORTION	8
2.2. CONCRETE TEST RESULTS	9
2.3. STEEL REINFORCEMENT	9
2.4. CFRP AND ADHESIVE	10
2.5. SPECIMEN DESIGN	10
2.6. CASTING R.C. BEAMS.....	11
2.7. PRE-LOADING.....	11
2.8. CFRP STRENGTHENING	12
2.9. INSTRUMENTATION	12
EXPERIMENTAL RESULTS AND DISCUSSION	13
MODE OF FAILURE AND CRACK PATTERNS	14
LOAD-DEFLECTION CURVE	15
STRAIN CHARACTERISTICS.....	16
DUCTILITY, TOUGHNESS, AND STIFFNESS	16
COMPARISON WITH ACI 440.2R	17
FEM ANALYSIS	21
CONSTITUTIVE MATERIAL	21
MESHING	23
INTERACTIONS	23
CFRP AND CONCRETE INTERFACE	23
LOADING AND BOUNDARY CONDITION	25
F.E. RESULTS.....	26
CONCLUSION	27
AUTHOR BIOGRAPHIES.....	28
REFERENCES	28
LIST OF TABLES	31
LIST OF FIGURES	32
TABLES	34
FIGURES.....	39

Introduction

Many reinforced concrete (R.C.) structures are damaged. Most of them are suffering from various deteriorations: cracks, concrete spalling, and large deflection. Many factors are at the origin of these deteriorations, such as aging, corrosion of steel, earthquake, environmental effects, and accidental impacts on the structure (Benjeddou, Ouezdou, & Bedday, 2007; Fayyadh & Abdul Razak, 2012).

Nowadays, it is vital to develop repair solutions that are both low-cost and quick to process. Externally bonded fibers reinforced polymers (FRP) has emerged as a new structural strengthening technology in response to the increasing need for repair and strengthening of reinforced concrete structures because of their high tensile strength, lightweight, resistance to corrosion, high durability, and ease of installation (Fayyadh & Abdul Razak, 2012; Lee & Hausmann, 2004).

The FRP is characterized by high-strength fibers embedded in polymer resin. Carbon, aramid, or glass fibers are the most prevalent types of FRP used in the industry. Repairing beam structures by externally bonded FRP composites consists of adhering FRP laminates at the tensile face of the beam. Among these types of FRP, the application of carbon fiber reinforced polymer (CFRP) to strengthen and repair the concrete beams has received the most attention from the research community (Benjeddou et al., 2007; Fayyadh & Abdul Razak, 2012; Lee & Hausmann, 2004).

The most published work on damaged R.C. beams repaired by FRP dealt with repairing these structures damaged by the corrosion effect. However, several numbers of research have been carried out on the retrofitting of the pre-damage R.C. beam due to overloading.

(Duarte, Correia, Ferreira, Nunes, & Arruda, 2014) Carried out experimental work on six T-shaped full-scale R.C. beams. The R.C. beams were pre-damaged based on the crack width of 0.3mm without yielding the steel reinforcement. Furthermore, the damaged R.C. beams were repaired using carbon fiber reinforced polymer ($E=165$ GPa and $f_u=1000$ MPa). After testing the R.C. beams using four-point static

loading, the authors concluded that the damaged R.C. beams increased their ultimate capacity and stiffness by %34 and %65, respectively, after strengthening compared to the control beams. In terms of ductility, all the repaired R.C. beams failed by debonding of CFRP; thus, the ductility was decreased compared to the control beams. Moreover, in comparison to the control beams, strengthened beams exhibited a much lower increase in crack width. This is due to the increased CFRP tensile reinforcement.

(Benjeddou et al., 2007) carried out an experimental investigation on six normal strength R.C. beams with the same reinforcement detailing and concrete strength. Three of the R.C. beams were tested as controlled beams, and they failed in flexure. The three others were pre-loaded damage beams up to %70 of the ultimate load of the control beams. In conclusion, the damage beams increased their load-carrying capacity by 17% when strengthened with a 100 mm width and 1.2mm thick of the CFRP sheet in a single layer compared to the control beam. Furthermore, the first flexural cracks of the strengthened appear at a higher load.

(Thanoon, Jaafar, Kadir, & Noorzaei, 2005) Has reported the structural performance of initially cracked R.C. one-way slabs strengthened with different techniques. Initially, all the slabs loaded to $(2/3)$ of their expected ultimate load capacity except for the control slab, which was loaded until failure. The pre-cracked R.C. slabs were repaired with five different techniques. The researchers used grout pouring S2, epoxy injection S3, ferrocement S4, CFRP strips S5, and section enlargement S6 as strengthening techniques. The R.C. slab S5 was strengthened using a 50mm wide CFRP strip externally bonded to the tension face of the R.C. slab. It was concluded that the ultimate load capacity of slab S5 showed a %77.4 higher ultimate load capacity than the control slab. The specimen reinforced with the carbon fiber strip shows no change in the initial stiffness compared to the control slab. With the loading increase, the stiffness decreases at a higher rate than specimens S1, S2, S3, and S4. Hence, the CFRP strip significantly affects the stiffness in the advanced stage of loading. Moreover, concrete compressive strain at mid-span at a distance of 25mm below the top fiber of R.C. slab specimens was recorded. All the slab specimens

exhibit lower strain values compared to the control slab. The decrease in the concrete strain in slab S5 has been recorded at 65%. The failure mechanism in Slab S5 is characterized by the shearing of the concrete interface with the CFRP strip (relative slippage) associated with less warning compared to other slab specimens. The failure was sudden and occurred immediately after the peeling of the CFRP strips; this is due to the insufficient anchorage length of the CFRP strip. The strain measured before failure in the CFRP laminate is 60% of its yielding strain, which complies with peeling failure (and not rupture failure) observed in this specimen. The number of cracks observed at failure is more, but the width of the crack is smaller compared to other specimens. The ductility performance for slab S5 was less than that of the control slab.

(Benjeddou et al., 2007) investigated the flexural behavior of repaired R.C. beams using CFRP laminates and the contribution of CFRP laminates to restore the strength and rigidity of the repaired beams. The main parameter of their work was the damage degree, which has been taken as (0%, 80%, 90%, and %100) of the ultimate load capacity of the control beam. The authors observed that repairing damaged R.C. beams with externally bonded CFRP laminates was successful for different degrees of damage. Therefore, this technique effectively restores the mechanical performance of cracked or damaged R.C. beams. The control beam failed due to steel yielding, resulting in a significant deflection of the beam and adequate ductility; nonetheless, the authors observed two failure mechanisms in all repaired beams: peeling off and interfacial debonding, both of which are brittle and abrupt failures. The authors concluded that all the repaired R.C. beams had a mechanical behavior in terms of load capacity and rigidity higher than that of the control beam. In addition, it was concluded that, for any damage degree, the CFRP laminates provide the repaired R.C. beam higher mechanical performances. The load capacity increases by 87% and 44% for damage degree 0% and 100%, respectively. The beam RB4 was completely damaged (pre-cracked to failure and large deflection: 10 mm), the contribution of CFRP laminate on the load capacity was very significant (144%). Furthermore, 80% and the 0% damage degree

beams behaved likely, and they gave a higher performance in terms of load capacity and rigidity due to the additional contribution of the reinforced concrete. Finally, there was no rupture of the CFRP laminates for all repaired beams due to the lack of end anchorage.

(Fayyadh & Abdul Razak, 2012) assessed the effectiveness of CFRP repaired R.C. beams under different damage levels. The experiments were carried out on scaled beams, with four beams serving as the datum. The first beam (D.B.) had no CFRP sheets, the second was a repaired beam after pre-damaging under design load limit (RBD), the third was a repaired beam after pre-damaging under steel yield load limit (RBY), and the fourth was a repaired beam after pre-damaging under ultimate load limit (RBU) (RBU). The study used the flexural stiffness change based on the secant modulus of the load against deflection curves for comparison. Comparisons were made based on the flexural stiffness recovery, crack patterns, load capacity, and failure modes of the beams. The results showed that regardless of the pre-repair damage level, and even if it is 100%, repairing with CFRP will be effective and increase the ultimate capacity by at least 147%. Furthermore, results showed that enhancing the flexural stiffness and load capacity would be smaller with the increase in the pre-repair damage level. The CFRP repair technique increases the load capacity regardless of the pre-repair damage level, where it increases the load capacity by 83%, 56%, and 48% for the pre-repair damage levels of 35%, 66%, and 100%, respectively. It has been noted that the CFRP repair technique recovers the stiffness and increases it further than the undamaged stiffness, whereby it increases the stiffness by 17%, 10%, and 4.6% for the pre-repair damage levels of 35%, 66%, and 100% respectively. Finally, they concluded that failure modes are governed by the pre-repair flexural cracks, which induce an intermediate crack at the adhesive layer, thus causing CFRP debonding.

(Lee & Hausmann, 2004) investigated the load capacity, ductility, and energy absorption aspects of R.C. beams retrofitted after damage with sprayed-fiber reinforce polymer composites (SFRP). SFRP consists of randomly oriented chopped fibers of controlled length in a polymer matrix. The results

indicated that SFRP could substantially increase strength and ductility and effectively strengthen and repair R.C. beams. Besides, it was concluded that carbon fibers lead to a higher increase in load-carrying ability and a lower increase in energy absorption for both damaged and undamaged R.C. beams due to their brittle characteristics compared to E-glass fibers.

(Aldahdooh, Muhamad Bunnori, Megat Johari, Jamrah, & Alnuaimi, 2016) developed a new green retrofitting material, called Green-USM-Reinforced Concrete (GUSMRC). The characteristics of this material (high tensile and flexural strengths) are very close to CFRP, which makes it suitable for retrofitting existing damaged concrete structures. Their study investigated the flexural behavior of damaged concrete beams caused by overloading when retrofitted by precast GUMSRC strips. The R.C. beams were damaged based on the ultimate load capacity of the control beams (25%, 50%, and 75%) and then rehabilitated. It was concluded that all retrofitting configurations significantly improved the strength of the beams in terms of a considerable increase in failure load.

By contrast, the mid-span deflection of retrofitted beams significantly decreased compared to the control beams, which had the highest deflections. Moreover, the effects of retrofitting at different damage levels were nearly the same.

(Morsy, El-Tony, & El-Naggar, 2015) Carried out an experimental investigation on the effect of using embedded CFRP rod as Near-surface Mounted (NSM) reinforcement for strengthening and repairing R.C. beams damaged by loading to different loading levels (0%, 50%, 70%, and 100% of ultimate load) and the results were compared with non-preloaded beams. Based on their findings, all the pre-loaded beams have lower stiffness than the control beams without pre-loading. However, the results indicated that the FRP reinforcement delays the crack propagation in the beams. The pre-loading levels have a minor effect on R.C. beams' enhancement capacity, as beams pre-loaded to 50% and 70% show a decrease in enhancement level by 4.2% compared with strengthened beam without pre-loading, which could be neglected.

This research aims to examine the flexural behavior and structural performance of pre-damaged reinforced concrete beams due to overloading, rehabilitated with externally bonded carbon fiber reinforced polymer (CFRP).

Research Significance

The majority of study has been conducted on pre-damage R.C. beams owing to heat or corrosion; few studies on pre-damage R.C. beams due to overloading are known. ACI 440.2R does not take the pre-damage level into account when calculating the moment capacity of FRP reinforced R.C. beams. The purpose of this study is to conduct an experimental and analytical examination of the influence of pre-damage level on the strength of CFRP reinforced R.C. beams.

Experimental work

Six reinforced concrete beams with the same cross-section and span are cast and tested under four-point bending. The R.C. specimens are pre-loaded to certain levels of strain in the main tensile reinforcement bars and then strengthened by a CFRP sheet. The materials used to cast R.C. beams are sand, gravel, water, cement, and reinforcement bars. Moreover, carbon fiber reinforced polymer (CFRP) and epoxy resin were used to externally strengthen the R.C. damage beam. The properties of the materials obtained from testing in the lab based on ASTM and from Manufacture suppliers are presented in the following sections.

2.1. Concrete mix proportion

River sand from Derbandi Ranya with 2.64 specific gravity and 2.91 fineness modulus was used for the trail mix. In addition, the percentage of absorption is 1.432%. River gravel obtained from Peramagrün is used for the mixed proportions. The specific gravity, dry rodded unit weight, percentage of absorption, and nominal maximum aggregate size are 2.63, 1647 kg/m³, 1.31%, and 12.5mm,

respectively. Ordinary Portland Cement (OPC) obtained from the Tasluja factory is used. Ordinary tap water was used for the mix proportions and curing of the specimens. The prepared materials (cement, sand, gravel, admixture, and water) were used to obtain trial mixes. The trial mixes for normal strength concrete were executed according to (ACI 211.1, 2002) based on the targeted compressive strength and workability. The sequence of mixing the materials and mixing time are essential keys to obtain a homogenous mix. The mixing sequence was as follows: first, the coarse aggregate was added inside the rotary mix, then half of the required water was added; second, all the fine aggregate was added to the mixer, followed by the cement. Finally, the remaining water was added gradually until a homogenous mixture was obtained. For NSC, the materials were mixed for 3 minutes, followed by 3 minutes rest, followed by 2 minutes mix again. Table 1 illustrates the selected mix proportions for casting R.C. beams. Table 2 shows the weight per cubic meter of each material used in the chosen mix proportion.

2.2. Concrete test results

Table 3 illustrates the average value of the mechanical properties of the concrete specimens. A set of cubes, cylinders, prisms were tested according to ASTM standards and EN BS standards in order to acquire cylindrical and cubical compressive strength, splitting tensile strength, modulus of rupture, and modulus of elasticity. The cylinders were capped according to (ASTM C617/C617M, 2012).

Figure 1 shows the concrete's stress-strain behavior obtained by installing two 80mm gauge length strain gauges on two opposite sides of the (150mm x 300mm) cylinder under compression. The concrete's modulus of elasticity (E) was measured under compression, using compressometer according to (ASTM-C469, 2002), as shown in Figure 2.

2.3. Steel reinforcement

Samples of deformed steel bars used for main tensile reinforcement and stirrups in the R.C. beams were prepared and tested according to (ASTM-E8/E8M-16a, 2016). The steel bars were obtained from

the Mass factory. Extensometer was installed on the samples with the universal tensile machine to obtain the stress-strain curve of each bar and measure the modulus of elasticity, as shown in Figure 3. Moreover, two strain gauges were installed on the samples to verify the results from the extensometer. Table 4 illustrates the measured diameter and mechanical characteristics of 8mm and 10mm bars.

2.4. CFRP and adhesive

ASOFABRIC-C300 carbon fiber fabric with ASODUR-1330 two components (A and B) epoxy adhesive products of AB-SCHOMBURG was used to strengthen the pre-damage R.C. beams. The carbon fiber fabric has 50cm width, and 100m length rolled, as shown in Figure 4. Table 5 illustrates the CFRP and epoxy adhesive properties based on the technical datasheet.

2.5. Specimen design

All the R.C. beams have the same cross-sections and spans (150mm x 250mm x 1800mm). R.C. beams were designed according to (ACI 318M, 2019) and intentionally oversized in shear so that the specimens will fail in flexure. The study parameter is pre-damage level, as presented in

Table 6 with the corresponded beam labels. Figure 5 shows the longitudinal section and cross-sections of the R.C. beams. The top bars were discontinued to the constant moment region so that the compression force will be resisted by the concrete only.

2.6. Casting R.C. beams

Six plywood molds and reinforcement cages were constructed and prepared for casting the R.C. beams, and 25mm plastic covers were used for the bottom and side cover of the reinforcement bars. The plywood molds were oiled before concrete casting to protect the molds and remove the molds easily after concrete hardening. A laboratory rotary mixer was used for mixing the materials. An electrical vibrator was used to vibrate and compact the fresh concrete in the molds to minimize air voids and segregations.

After the concrete was cast, the top surface of the fresh concrete was leveled and smoothed. The R.C. beams were left for 24 hours in the molds covered with wet gunny sacks. The hardened R.C. beams were removed from the molds and water cured for seven days and left for 28 days before the pre-loading process in order to gain full concrete strength. The R.C. beams were painted using white color water emulsion painting and labeled using the marker. The reason for the painting is to notice the crack when it occurred.

2.7. Pre-loading

All the R.C. beams except for B1 and B2 were loaded and damaged before strengthening. The damage levels were based on the strain in the main tensile bars of the R.C. beams. Four different damage levels were conducted depending on the certain strain in the tensile bars. B3 was damaged up to 1800 microstrain; however, B4 was damaged up to yield strain of the main bar. Moreover, B5 was loaded up to 3000 microstrains, and B6 was loaded up to 4000 microstrains. Figure 6 shows loading and unloading versus strain of the R.C. beams before strengthening.

Figure 7 shows crack patterns for R.C. beams with different damage levels. The cracks are flexural as expected because the R.C. beams are over-designed in shear. The first crack occurred under one of the point loads. For B3 and B4, the first crack appeared around 14kN and 16kN, respectively. Furthermore, as it is obvious in the load-strain relation for B5 and B6, the first crack occurred at a load of 21kN.

2.8. CFRP strengthening

Before applying CFRP and epoxy resin on the concrete tension face, dust, piece of extra concrete, water emulsion paint, and moisture should be removed using a mechanical grinder and brush. Therefore, the R.C. beams were overturned on the bottom surface. The surface was washed using water and dried using an air blower before CFRP application.

The pre- damaged R.C. beams were strengthened with 150mm width of one layer of CFRP in the tension face. The two-component resin A and B were mixed and applied on concrete surfaces and CFRP sheets, and then the saturated CFRP sheet was applied on the concrete surface. A wooden roller was slowly used to press out air and extra resin. Based on the manufacturer's technical report, the strengthened beams were left for 28 days in the laboratory to harden the epoxy resin.

2.9. Instrumentation

Figure 8 shows a schematic representation of the loading setup and instrumentation. The strengthened R.C. beams were tested under four-point bending using a hydraulic jack of 800kN capacity. The pressure from the jack is divided into two-point loads using an I-section steel beam with two load cells of 300kN capacity each. Four steel plates (60mm x 200mm x 20mm) were used under the load cells and on the supports to prevent local failure due to stress concentration.

Three different gauge lengths of strain gauges were installed, 3mm strain gauges installed on the main tensile bars at mid-span and on the fourth stirrup from the support to read the tensile strain of the bars. 10mm strain gauges were installed on the CFRP sheets at mid-span and near the supports to measure the tensile strain of the CFRP sheet. Furthermore, 80mm strain gauges were installed on the top, top face, and bottom of the concrete section at mid-span to measure the top compressive strain and bottom tensile strain of the concrete.

Five LVDTs (Linear Variable Differential Transformer) were used to measure the deflection at mid-span, under the point load, and mid-way between the point load and the right support and to measure top concrete compressive strain and bottom tensile strain.

Windmill MicroLink 851 data logger with 594 box (screw terminals with strain measurement) were used to collect and read the load cells, LVDTs, and strain gauges.

Experimental results and discussion

Five R.C. beams (B2-B6) with different pre-loading levels were tested to investigate the effect of different pre-damage levels on the failure mode, crack pattern, load-deflection curve, strain contribution of CFRP, and ductility of the CFRP strengthened R.C. beams. The specimen B2 is strengthened without pre-loading; B3, B4, B5, and B6 were pre-loaded up to %53.7, %81.2, %84.5, and %97.4 of the ultimate load capacity of the control beam before FRP strengthening.

Figure 9 shows the loading and unloading process and the load-deflection curve of the strengthened R.C. beams after damage. The test results of the strengthened R.C. beams are compared with the control beam B1.

Mode of failure and crack patterns

The control beam experienced a flexure crack mostly under and between the point loads (constant moment region) and propagated towards the support, as shown in Figure 10. With increasing the applied load, top concrete fibers reached the ultimate strain, and the control beam failed in concrete crushing after yielding the steel bars, as shown in Figure 11, which is a typical tension control failure according to ACI-318. Before the failure, B1 underwent deflection and had ductile behavior.

Furthermore, the strengthened R.C. beams (B2-B6) suffered from more flexure cracks than B1 before failure; as shown in Figure 10, the width of the old cracks was increased, and the new cracks appeared. The cracks initiated under the point load and distributed along the R.C. beams. Moreover, the cracks propagate towards the compression region, especially in beams B5 and B6; more cracks reached the compression region. At the final stage of loading before failure, some diagonal cracks, indicating shear cracks, near the supports initiated in the strengthened R.C. beams due to the increase in the flexure capacity of CFRP reinforced beams.

All the strengthened R.C. failed in FRP debonding; FRP debonding was initiated near the supports and propagated toward mid-span. Before CFRP debonding, the epoxy resin fractured because of reaching its tensile capacity.

The beams B2-B4 failed in CFRP end peeling off, as shown in Figure 11, without cover delamination. However, as shown in Figure 11, specimens B5 and B6 failed in concrete cover delamination; this might be because the concrete cover was weakened since the concrete surface was more damaged and encountered broad cracks during the pre-loading procedure prior to applying CFRP. Cover delamination occurred under one of the point loads in which a part of concrete was separated from the R.C. beams attached to the FRP, and the reinforced bar appeared, as shown in Figure 12. After FRP debonding, loading was continued until concrete crushing occurred.

Load-deflection curve

Table 7 presents the load and mid-span deflection of specimen B1-B6 at critical loading stages. The first crack of specimen B1 occurred at a load of 14.3kN with a corresponded mid-span deflection of 1.79mm. However, in specimen B2, the first crack occurred at a higher load of 26.8kN with a lower corresponded mid-span deflection of 1.36mm. Thus, it can be concluded that CFRP delays the first crack and increases the cracking load by 87.4%. Furthermore, in the strengthened R.C. beams, the steel bar yields at a higher load than B1; for instance, in B2, the steel yielding load increased by 34.4%.

All the strengthened R.C. beams, B2-B6, have higher ultimate load capacity and lower mid-span deflection than specimen B1, as shown in Figure 13 and Figure 14. For beams B2-B6, the ultimate load capacity was increased by 64%, 59%, 67%, 62%, and 56%, respectively. However, the mid-span deflection at failure for beams B2-B6 was decreased by 62%, 67%, 63%, 56%, 70%, respectively. Specimen B4 has the highest ultimate load among all the strengthened R.C. beams, and specimen B6 has the lowest capacity. It may be deduced that the increase in the CFRP reinforced beams' ultimate load capacity is independent of the pre-loading level.

The post debonding behavior of the strengthened R.C. beams was similar to the behavior of the control beam. Figure 15 shows the mid-span deflection curves of specimen B1-B6 at different load levels. The mid-span deflection of B2-B6 was lower than B1 at first crack load, the yield of steel load, and ultimate load because CFRP increases the flexure rigidity of the R.C. beams. However, after CFRP debonding, the strengthened R.C. beams have more deflection up to concrete crushing than the control beam because the strengthened R.C. beams experienced more and wider cracks before debonding, and the R.C. beams lost most of the flexure rigidity after CFRP debonding.

Strain characteristics

Table 8 presents the strain in the top concrete fiber, steel bars, and CFRP sheet at mid-span at failure. Figure 16 illustrates the load-strain curve of concrete, tensile steel bar, and CFRP sheet.

The yielding strain of the steel bar is 2400 microstrain, so the steel bars yielded before failure in all the R.C. beams. Because some of the strain gauges were damaged or did not read the value properly, the strain result is not presented. Since the concrete crushing for B1 occurred near the right point load, the top concrete strain gauge did not reach the strain failure of concrete at mid-span. Similarly, for B3, the steel strain gauge provided a higher value because the wider flexure crack occurred at mid-span.

The rupture tensile strain of CFRP (ϵ_{fu}) provided by the manufacture datasheet is 21000 microstrain. In all the CFRP strengthened beams, CFRP strain at debonding was between 41.2%-33% of the FRP rupture strain. B2 gives the highest CFRP strain before debonding; however, B6 gives the lowest CFRP strain. The strain contribution of CFRP decreases with increasing the damage level. For B2 with zero damage level, the CFRP strain reached 41.2% of the CFRP rupture strain. The ratio of CFRP strain to the strain of rupture for B3, B4, and B5 were approximately the same 36.4%, 38.2%, and 38.7%, respectively. Beam B6, with a higher damage level, gives the lowest ratio, 33%.

Ductility, toughness, and stiffness

Table 9 and Figure 17 illustrate the toughness, ductility, performance factor, and initial stiffness of the R.C. beams. Toughness is the area under the load-deflection curve up to failure. Specimen B1 gives the highest area under the curve, which means it has a ductile behavior so that energy could be dissipated. On the other hand, the strengthened beams B2-B6 provide approximately similar toughness and dissipate energy less than B1 because the failure was controlled by CFRP debonding.

In addition, B1 has more ductility than the strengthened R.C. beams, which was apparent during the loading test. Ductility is the ultimate deflection divided by deflection at the yield of the steel bars. The ductility of beams B2-B6 was reduced by 39%, 36%, 39%, 27%, and 46%, respectively. Furthermore, B2, B3, and B4 have similar ductility. Also, B5 has the highest ductility of 2.71 among all the strengthened R.C. beams. However, specimen B6, with the highest pre-damage level, has the lowest ductility of 2.

Bonding CFRP to the concrete surface increases the initial stiffness of the strengthened R.C. beams because CFRP has a high modulus of elasticity. Specimen B2 has the highest initial stiffness of 30.5kN/mm; however, B1 has the lowest initial stiffness of 10.3kN/mm. B3, which is pre-damaged up to before steel bar yield, has nearly similar stiffness (28.8kN/mm) to B2. The initial stiffness of B2, B3, B4, B5, and B6 are increased by 196%, 180%, 128%, 90%, and 78% compared to the initial stiffness of B1, respectively.

Increasing the damage level reduces the initial stiffness of the strengthened R.C. beams, as shown in Figure 18, because the concrete is cracked, and the steel bar is stressed before CFRP bonding. B3, B4, B5, and B6 reduced their initial stiffness by 5.6%, 23%, 36%, and 40%, respectively, as compared to B2.

The performance factor is the product of the ductility factor and strength factor. All the R.C. beams have approximately similar performance factors greater than one except for B6, which has the lowest performance factor, less than one.

Comparison with ACI 440.2R

FRP reinforcing systems should be designed to withstand tensile stresses while being strain compatible with the concrete substrate. The design suggestions in (ACI committee 440, 2004) are based

on traditional reinforced concrete design concepts as described in ACI 318-05 criteria and understanding of the particular mechanical behavior of FRP reinforcement.

The constituent materials, fibers, and resins of an FRP system affect its durability and resistance to environmental exposure. Table 10 illustrates environmental reduction factors for the various FRP systems and exposure conditions. The reduction factor is closer to one if the FRP system is placed in a generally non-threatening environment, such as indoors. If the FRP system is exposed to high humidity, freezing, and thawing cycles, saltwater, or alkalinity for an extended period of time, a smaller reduction factor should be utilized.

Equations 1 through 3 give the tensile properties that should be used in all design equations. The design ultimate tensile strength and rupture strain should be reduced for environmental exposure conditions.

Hooke's law may be used to estimate the design modulus of elasticity for unidirectional FRP since FRP materials are linear elastic until they fail. The modulus of elasticity statement in equation 3 acknowledges that the modulus of elasticity is usually unaffected by environmental factors.

$$f_{fu} = C_E f_{fu}^* \quad 1$$

$$\varepsilon_{fu} = C_E \varepsilon_{fu}^* \quad 2$$

$$E_f = f_{fu} / \varepsilon_{fu} \quad 3$$

FRP debonding or cover delamination occurs in the majority of externally bonded FRP systems.

To avoid a debonding failure mode, the effective strain in FRP reinforcement should be restricted to the debonding strain level, ε_{fd} , as stated in equation 4.

$$\varepsilon_{fd} = 0.41 \sqrt{\frac{f'_c}{n E_f t_f}} \leq 0.9 \varepsilon_{fu} \quad 4$$

A trial-and-error technique is illustrated in the calculating procedure provided in (ACI committee 440, 2004). Choosing an assumed depth to the neutral axis c , computing the strain level in each material using strain compatibility, calculating the related stress level in each material, and confirming internal force equilibrium are all part of the trial-and-error procedure. If the internal force resultants do not attain equilibrium, adjust the depth to the neutral axis and repeat the operation. At the ultimate limit condition, Figure 19 depicts strain compatibility, stress distribution, and forces equilibrium for a rectangular segment strengthened by FRP.

Equations 5 and 6 calculate the effective strain and effective stress in the FRP, respectively. In equation 5, ε_{bi} is the initial substrate strain, equal to zero in our case because the R.C. beams were unloaded and upturned before applying the CFRP sheets. Concrete crushing limits flexural failure of the section if the left term of the discrepancy is controlled. FRP rupture or debonding governs flexural failure of the section if the right term of the inequality controls.

$$\varepsilon_{fe} = \varepsilon_{cu} \left[\frac{d_f - c}{c} \right] - \varepsilon_{bi} \leq \varepsilon_{fd} \quad 5$$

$$f_{fe} = E_f \varepsilon_{fe} \quad 6$$

Equations 7 and 8 are used to compute the strain and stress in tensile steel bars, respectively. The neutral axis is calculated using equation 9, α_1 and β_1 are the values related to the Whitney stress block ($\alpha_1 = 0.85$ and β_1 from ACI 318-05).

The procedure is repeated until the equilibrium of the internal forces and strain compatibility are satisfied.

$$\varepsilon_s = (\varepsilon_{fe} + \varepsilon_{bi}) \left[\frac{d - c}{d_f - c} \right] \quad 7$$

$$f_s = E_s \varepsilon_s \leq f_y \quad 8$$

$$c = \frac{A_s f_s + A_f f_{fe}}{\alpha_1 f'_c \beta_1 b} \quad 9$$

Equation 10 is used to calculate the nominal flexural strength of the section with FRP external reinforcement. The flexural strength input of the FRP reinforcement is reduced by a factor called ψ_f . The strength reduction factor, ψ_f , is used to increase the accuracy of strength predictions by accounting for the various failure modes seen in FRP-strengthened components (delamination of FRP reinforcement). The suggested value for ψ_f is 0.85.

$$M_n = A_s f_s \left[d - \frac{\beta_1 c}{2} \right] + \psi_f A_f f_{fe} \left[d_f - \frac{\beta_1 c}{2} \right] \quad 10$$

Table 11 and Figure 20 illustrate the comparison between the ultimate analytical load obtained from (ACI committee 440, 2004) and experimental ultimate load capacity. It can be concluded that ACI 440 predicts the ultimate load capacity marvelously for externally bonded FRP beams compared to the experimental ultimate load capacity.

Because the ACI 440 does not consider the effect of the pre-damage level in the computation of the flexure strength of the FRP strengthened R.C. beams, some variances are noticed.

FEM analysis

The R.C. beams were modeled for finite element analysis using ABAQUS CAE, and the results are validated based on the experimental results. Four solid plates with (60mm x 20mm x 200mm) dimensions were used to model the loading plates and the supports. The plates were modeled as pure elastic behavior using ($E= 200\text{GPa}$).

Constitutive material

The material properties obtained from the experimental test were used to model the concrete and the steel reinforcement. CFRP sheet was modeled as linear elastic isotropic up to failure with the same data obtained from the manufacture datasheet presented in section 2.4. . Furthermore, the stress-strain curve of the steel reinforcement obtained from the experimental test, as presented in section 2.3, was used to model the steel reinforcement properties.

The concrete constitutive models implemented in ABAQUS include the Concrete Smeared Cracking model and the Concrete Damaged Plasticity model. Concrete Damaged Plasticity (CDP) is a powerful tool to model the plastic behavior of concrete. CDP includes plasticity, compressive behavior, and tensile behavior.

Table 12 illustrates the final value of the parameters used to model the plasticity of the concrete after verification with the experimental results.

Because the descending part of the compressive stress-strain curve could not be achieved experimentally, (Chin & Mansur, 1996) model is used to model the compressive behavior of the concrete. Equations 11 through 13 and Figure 21a present the concrete compressive behavior. The model is chosen based on the compatibility of the ascending part of the experimental stress-strain curve with the model.

$$f_c = f'_c \left[\frac{k_1 \beta \left(\frac{\varepsilon}{\varepsilon_0} \right)}{k_1 \beta - 1 + \left(\frac{\varepsilon}{\varepsilon_0} \right)^{k_2 \beta}} \right] \quad 11$$

$$k_1 = \left(\frac{50}{f'_c} \right)^{3.0}, \quad k_2 = \left(\frac{50}{f'_c} \right)^{1.3} \quad 12$$

$$\beta = \frac{1}{1 - \left(f'_c / \varepsilon_0 E_{it} \right)} \quad 13$$

Furthermore, (Sneed, Dere, & Koroglu, 2017) model is used to model the tensile behavior of the concrete. Equation 14 and Figure 21b illustrate the tensile behavior of the concrete.

$$\sigma = f_t \left(\frac{\varepsilon_t}{\varepsilon} \right)^{(0.7+1000\varepsilon)}, \quad \varepsilon_t = \frac{f_t}{E_c} \quad 14$$

Meshing

The R.C. beams had been optimized using mesh sensitivity and chosen meshing size of 20mm was found to best approximate the overall structural response of the examined beams and less time-consuming.

An 8-node linear brick, reduced integration, hourglass control (C3D8R) element type is assigned to the concrete and loading plates. Furthermore, a 2-node linear beam in space (B31) element type is set to the reinforcement cage. Finally, a 4-node doubly curved thin or thick shell, reduced integration, hourglass control, finite membrane strains (S4R) is assigned to the CFRP sheet.

Interactions

The interaction between the concrete and steel reinforcement and the R.C. beam and the loading plates should be defined in ABAQUS. The embedded region was used to assume a complete connection between the concrete and steel reinforcement. In the embedded region, the concrete is the host, and the steel reinforcement is the embedded region. The perfect bond assumption may lead to higher stiffness of the model in the load-deflection curve response than the experimental. Furthermore, a perfect bond between the loading plates and the R.C. beam is assumed using Tie contact. The R.C. beam is the master surface; however, the loading plates are the slave surface.

CFRP and concrete interface

The model for the interface between FRP and concrete is of essential importance. A perfect bond model and cohesive models were evaluated for describing the concrete-FRP interface. The ultimate load and stiffness were overestimated with a perfect bond between FRP, and concrete compared to experimental results. This is because degradation in the bond cannot be captured in this type of model, and it implies that a perfect bond model is not suitable in a study focusing on debonding.

The cohesive model available in ABAQUS is a better choice for representing the interface behavior. The cohesive model defines surfaces of separation and describes their interaction by defining a relative displacement at each contact point. The initial stiffness, shear strength, fracture energy, which is equal to the area under the traction–displacement curve, and the curve shape of the bond-slip model are the parameters that define the model. Figure 22 shows a graphic interpretation of a simple bilinear traction–separation law written in terms of the effective traction τ and effective opening displacement δ , as recommended by (Obaidat, 2011).

In previous models, the input data was only related to the concrete properties, and it was considered necessary also to include the adhesive properties.

The following relations 15 through 17 for initial stiffness, shear strength, and fracture energy, as a function of the adhesive and concrete properties, were recommended by (Obaidat, 2011):

$$K_{nn} = \frac{1}{\frac{t_c}{E_c} + \frac{t_{epoxy}}{E_{epoxy}}} \quad 15$$

Where; K_{nn} is normal stiffness from peeling off test, t_c is the concrete thickness= 5 mm, t_{epoxy} is the epoxy or adhesive thickness =1 mm, E_c = Young's modulus of concrete, and E_{epoxy} = Young's modulus of adhesive. The approximate value of $K_{nn} = 1700$ MPa.

$$K_{ss} = K_{tt} = \frac{1}{\frac{t_c}{G_c} + \frac{t_{epoxy}}{G_{epoxy}}} \quad 16$$

Where, $K_{ss}=K_{tt}$ = shear stiffness from lap joint test, G_c = Shear modulus of concrete = 10800 MPa, G_{epoxy} = Shear modulus of epoxy or adhesive = 665 MPa.

$$\tau_{max} = 1.5 \times f_{ct} \times \sqrt{\left[2.25 - \frac{b_f}{b_c}\right] / \left[1.25 + \frac{b_f}{b_c}\right]}$$

Where, f_{ct} = Tensile strength of concrete, MPa, b_f = FRP plate width, mm, b_c = Concrete width, mm.

The damage initiation was assumed to occur when a quadratic traction function involving the nominal stress ratios reached value one.

Interface damage evolution was expressed in terms of energy release. The description of this model is available in the Abaqus material library. The Benzaggah–Kenane fracture criteria was used to determine the fracture energy's dependency on the mode mix. Benzaggah–Kenane fracture criterion is particularly useful when the critical fracture energies during deformation are the same along with the first and second shear directions.

In order to find the values of initial stiffness, shear strength, and fracture energy that gave the best fit, simulations were performed, and the results were compared with experimental results. The shear strength has more effect on the debonding failure load and load-deflection curve than the other parameters. Table 13 presents the input value of the cohesive model.

Loading and boundary condition

Two static load points were applied at the loading plates corresponding to the experimental location using displacement control. The displacement increments were applied as a smooth step in the loading amplitude.

The boundary condition of the supporting plates was specified at the appropriate nodes as a simply supported beam. One plate has restrained the displacement in the X and Y direction representing

pin support, and the other plate has restrained the displacement only in the Y direction representing roller support.

When performing a nonlinear analysis, convergence difficulties may occur, especially when cracks start to initiate. In order to avoid convergence issues, dynamic explicit were used to perform nonlinear analysis.

F.E. Results

Figure 23 shows the first crack initiation of the control beam, B1. The first crack occurred at the load of 18.3 kN at the time step of 0.1 seconds, which is 87% of the load obtained in the experiment. Furthermore Figure 24 and Figure 25 show axial stress and axial strain in the steel reinforcement at failure, respectively. It can be seen that the steel reinforcement reaches yielding before concrete crushing occurs.

Figure 26 shows the flexure crack propagation in the control beam, B1. Also, Figure 27 shows the concrete compression failure of the control beam. The crack patterns and concrete crushing are well agreed with the experiment.

Figure 28 presents the CFRP debonding failure of the strengthened R.C. beams B2-B6. The debonding failure of the CFRP sheet can be well captured using the cohesive interface.

The load-deflection curves of the control beams and retrofitted R.C. beams obtained from the experiment and FEM analysis are illustrated in Figure 29. Because of the anticipated perfect connection between concrete and reinforcement, the FEM analysis indicates that the beam will be somewhat stiffer and stronger.

Table 14, Figure 30, and Figure 31 present the comparison between experimental and analytical ultimate load and mid-span deflection for the control beams and enhanced R.C. beams. It can be stated

that FEM and experimental data are in excellent agreement. The good agreement indicates that the constitutive models used for concrete and reinforcement and the cohesive interface model can well capture fracture behavior.

Conclusion

To conclude,

- The failure mode of the CFRP strengthened specimen was controlled by CFRP debonding followed by concrete crushing; however, the control failed in concrete crushing after yielding the steel bars, which is typical tension control failure according to ACI-318.
- The epoxy resin properties significantly influence the debonding failure because the epoxy resin ruptured in tension before CFRP debonding. So, improving the epoxy properties, predominantly tensile and flexure strength, enhances the bond strength and postpones the CFRP debonding.
- CFRP sheet restores and upgrades the strength and stiffness of the damaged R.C. beams; however, it reduces ductility and toughness. Also, CFRP application increases the first crack and yielding steel bars load by 87.4% and 34.4%, respectively.
- The pre-damage level does not influence the strength and ductility of the strengthened R.C. beams except for the highest damage levels, which experienced a slight decrease in load capacity and ductility. However, the initial stiffness decreases with increasing pre-damage levels by 40%.
- ACI 440.2R predicts the ultimate load capacity marvelously for externally bonded FRP beams compared to the experimental ultimate load capacity. Because the ACI 440 does not consider the effect of the pre-damage level in the computation of the flexure strength of the FRP strengthened R.C. beams, some variances are noticed.

- It can be concluded that there is a good agreement between FEM and experimental results for the control beams and strengthened R.C. beams. The good agreement indicates that the constitutive models used for concrete and reinforcement and the cohesive interface model can well capture fracture behavior. The FEM study, on the other hand, indicates that the beam will be somewhat stiffer and stronger, owing to the anticipated perfect connection between concrete and reinforcement.

Author Biographies

Brwa HS Hamah-Ali

Ph.D. and senior lecturer at civil engineering department, college of engineering, university of Sulaimani.

Brwa Hamah Saeed was appointed as an assistant lecturer in the civil department in April 2013. He studied master's degree in structural engineering with distinction at the University of Sheffield, UK, fully funded by the HCDP scholar program covered by KRG. Furthermore, he worked as a demonstrator in the department for two years. He also worked as a site engineer for more than two years in a wide range of engineering projects. Additionally, he accomplished a bachelor's degree in building construction at the University of Sulaimani in 2009, and he was ranked second.



References

- ACI 211.1, A. (2002). Standard Practice for Selecting Proportions for Normal, Heavyweight, and Mass Concrete (ACI 211.1-91). *Concrete*, (Reapproved), 1–38.
- ACI 211.4R, A. (2008). Guide for Selecting Proportions for High-Strength Concrete Using Portland Cement and Other Cementitious Materials, 29.
- ACI 318, A. (2019). Building code requirements for structural concrete (ACI 318-19) an ACI standard (SI unit), and Commentary (ACI 318R-19) Reported by ACI committee 318. Retrieved from <https://www.concrete.org/publications/internationalconcreteabstractsportal.aspx?m=details&ID=51716937>
- ACI committee 440. (2004). *Guide for the design and construction of externally bonded FRP systems for strengthening existing structures*. ACI committee 440.
- ASTM-C39M. (2014). Standard Test Method for Compressive Strength of Cylindrical Concrete

Specimens, 3–9. <https://doi.org/10.1520/C0039>

ASTM-C469. (2002). ASTM C469-02: Standard Test Method for Static Modulus of Elasticity and Poisson's Ratio of Concrete in Compression. *ASTM Standard Book, 04*, 1–5. Retrieved from [http://portales.puj.edu.co/wjfajardo/mecanica de solidos/laboratorios/astm/C469.pdf](http://portales.puj.edu.co/wjfajardo/mecanica%20de%20solidos/laboratorios/astm/C469.pdf)

ASTM-C78. (2002). Standard Test Method for Flexural Strength of Concrete (Using Simple Beam with, 1–3.

ASTM C496/C496M. (2011). Standard Test Method for Splitting Tensile Strength of Cylindrical Concrete Specimens ASTM C-496. *ASTM International*, (March 1996), 1–5. Retrieved from [ftp://ftp.astmtmc.cmu.edu/docs/diesel/cummins/procedure_and_ils/ism/Archive/ISM Procedure \(Draft 10\).doc](ftp://ftp.astmtmc.cmu.edu/docs/diesel/cummins/procedure_and_ils/ism/Archive/ISM%20Procedure%20(Draft%2010).doc)

ASTM C617/C617M. (2012). Standard Practice for Capping Cylindrical Concrete Specimens. *ASTM International*, 98(Reapproved), 1–6. <https://doi.org/10.1520/C0617>

ASTM-D3039/D3039M. (2017). Astm D3039/D3039M. *Annual Book of ASTM Standards*, 1–13. <https://doi.org/10.1520/D3039>

ASTM-E8/E8M-16a. (2016). Standard Test Methods for Tension Testing of Metallic Materials 1, *i*. <https://doi.org/10.1520/E0008>

Aldahdooh, M. A. A., Muhamad Bunnori, N., Megat Johari, M. A., Jamrah, A., & Alnuaimi, A. (2016).

Retrofitting of damaged reinforced concrete beams with a new green cementitious composites material. *Composite Structures*, 142, 27–34. <https://doi.org/10.1016/j.compstruct.2016.01.067>

Benjeddou, O., Ouezdou, M. Ben, & Bedday, A. (2007). Damaged R.C. beams repaired by bonding of CFRP laminates. *Construction and Building Materials*, 21(6), 1301–1310.

<https://doi.org/10.1016/j.conbuildmat.2006.01.008>

EN BS 12390-3, B. E. (2001). Testing hardened concrete-Part3: Compressive strength of test specimens.

Chin, B. T. H. W. M. S., & Mansur, M. A. (1996). STRESS-STRAIN RELATIONSHIP OF HIGH-

STRENGTH CONCRETE IN COMPRESSION, (May), 70–76.

- Duarte, P., Correia, J. R., Ferreira, J. G., Nunes, F., & Arruda, M. R. T. (2014). Experimental and numerical study on the effect of repairing reinforced concrete cracked beams strengthened with carbon fibre reinforced polymer laminates. *Canadian Journal of Civil Engineering*, *41*(3), 222–231. <https://doi.org/10.1139/cjce-2013-0124>
- Fayyadh, M. M., & Abdul Razak, H. (2012). Assessment of effectiveness of CFRP repaired R.C. beams under different damage levels based on flexural stiffness. *Construction and Building Materials*, *37*, 125–134. <https://doi.org/10.1016/j.conbuildmat.2012.07.021>
- Lee, H. K., & Hausmann, L. R. (2004). Structural repair and strengthening of damaged R.C. beams with sprayed FRP. *Composite Structures*, *63*(2), 201–209. [https://doi.org/10.1016/S0263-8223\(03\)00156-9](https://doi.org/10.1016/S0263-8223(03)00156-9)
- Morsy, A. M., El-Tony, E. T. M., & El-Naggar, M. (2015). Flexural repair/strengthening of pre-damaged R.C. beams using embedded CFRP rods. *Alexandria Engineering Journal*, *54*(4), 1175–1179. <https://doi.org/10.1016/j.aej.2015.07.012>
- Obaidat, Y. T. (2011). *STRUCTURAL RETROFITTING OF CONCRETE BEAMS USING FRP - Debonding Issues*.
- Sneed, L., Dere, Y., & Koroglu, M. A. (2017). Nonlinear F.E. Modeling of Reinforced Concrete Nonlinear F.E. Modeling of Reinforced Concrete. *International Journal of Structural and Civil Engineering Research*, *6*(February), 71–74. <https://doi.org/10.18178/ijscer.6.1.71-74>
- Thanoon, W. A., Jaafar, M. S., Kadir, M. R. A., & Noorzaeei, J. (2005). Repair and structural performance of initially cracked reinforced concrete slabs. *Construction and Building Materials*, *19*(8), 595–603. <https://doi.org/10.1016/j.conbuildmat.2005.01.011>

List Of Tables

<i>Table 1: Selected mix proportions for casting RC beams.</i>	34
<i>Table 2: Weight of the materials for 1m³ of the selected mix proportions.</i>	34
<i>Table 3: mechanical properties of the concrete beams.</i>	34
<i>Table 4: Mechanical properties of the reinforcement bars.</i>	35
<i>Table 5: Properties of CFRP and epoxy adhesive based on the technical datasheet.</i>	35
<i>Table 6: Details of the R.C. beams.</i>	36
<i>Table 7: Mode of failure and load and mid-span deflection at first crack, the yield of steel, and the ultimate stage.</i>	36
<i>Table 8: Strain of concrete, steel, CFRP at failure.</i>	37
<i>Table 9: Strength factor, stiffness, toughness, ductility factor, and performance factor.</i>	37
<i>Table 10: Environmental reduction factor for various FRP systems and exposure conditions (ACI committee 440, 2004).</i>	37
<i>Table 11: Experimental and Analytical comparison.</i>	38
<i>Table 12: Concrete Damaged Plasticity parameters.</i>	38
<i>Table 13: Parameters of the Cohesive contact between CFRP and concrete substrate.</i>	38
<i>Table 14: Experimental and FEM comparison of the R.C. beams.</i>	39

List of figures

Figure 1: Stress-Strain curve of NSC using strain gauges. _____	39
Figure 2: Modulus of elasticity test using compressometer. _____	39
Figure 3: Tensile test of steel bars using extensometer and strain gauges and stress-strain curve for 8mm and 10mm bar. _____	40
Figure 4: CFRP and epoxy resin: (a) CFRP roller; (b) epoxy resin component A; and (c) epoxy resin component B.	40
Figure 5: Longitudinal and cross-section of the R.C. beams. _____	41
Figure 6: Load-strain relation of the damaged R.C. beams. _____	42
Figure 7: Crack Pattern of R.C. beams after damage for different damage levels. _____	43
Figure 8: Loading setup and instruments. _____	44
Figure 9: Load-deflection curve for pre-damage and strengthened beams. _____	45
Figure 10: Crack patterns before failure. _____	46
Figure 11: Failure mode of the R.C. beams: concrete crushing, B1; FRP end peeling off, B2-B4; and concrete cover separation, B5 and B6. _____	47
Figure 12: Cover separation bottom view; (a) B5, and (b) B6. _____	47
Figure 13: Load-deflection curve. _____	48
Figure 14: Ultimate load and damage levels. _____	48
Figure 15: Deflection curve at critical loads. _____	49
Figure 16: Load-strain curve. _____	50
Figure 17: Stiffness increase, strength factor, ductility factor, and performance factor. _____	51
Figure 18: Stiffness and damage levels. _____	51
Figure 19: Internal strain and stress distribution for a rectangular section under flexure at ultimate limit state (ACI committee 440, 2004). _____	51
Figure 20: Relation between experimental and ACI 440 ultimate load capacity. _____	52
Figure 21: Concrete behavior: (a) compressive behavior, (b) tensile behavior. _____	52
Figure 22: Bond-slip curve, bilinear model (Obaidat, 2011). _____	53
Figure 23: First crack for specimen B1. _____	53

<i>Figure 24: Stress in the reinforcement steel for the B1.</i>	53
<i>Figure 25: Strain in the reinforcement steel for the B1.</i>	54
<i>Figure 26: Crack patterns for the B1.</i>	54
<i>Figure 27: Concrete compression failure in the B1.</i>	54
<i>Figure 28: CFRP Debonding for the R.C. beams.</i>	55
<i>Figure 29: Experimental and F.E. Load vs. mid-span deflection for the R.C. beams.</i>	56
<i>Figure 30: Relation between experimental and FEM load capacity of the R.C. beams.</i>	57
<i>Figure 31: Relation between experimental and FEM mid-span deflection of the R.C. beams.</i>	57

Tables

Table 1: Selected mix proportions for casting RC beams.

Mix Proportions	Types of Concrete	Mix Ratio C:S:G	W/C ratio	Cement kg/m ³	HRWR%*	F/C*	fc', MPa	Slump mm
I	NSC*	1:1.8:1.56	0.43	480	0.0%	1.140	45	100

*F/C: the ratio of fine to coarse aggregate.

*HRWR%: High Range Weight Reducer as a percentage of cement.

*NSC: Normal Strength Concrete.

Table 2: Weight of the materials for 1m³ of the selected mix proportions.

Mix Proportions	Weight kg/m ³				
	Cement	Water	Sand	Gravel	HRWR
I	480	216	854	748.8	0

Table 3: mechanical properties of the concrete beams.

Mechanical Properties	Results
	B1-B6
f'c (MPa)	43
fcu (MPa)	63
f'c/fcu	0.7
fr (MPa)	5.5
fsp (MPa)	3.9
E (GPa)	31

Table 4: Mechanical properties of the reinforcement bars.

Reinforcement bar	8mm			10mm		
	Mean	Standard Deviation	COV	Mean	Standard Deviation	COV
diameter (mm)	7.68	0.057	0.0074	9.77	0.0147	0.0015
fy (MPa)	330	28.46	0.0862	573	11.49	0.0201
fu (MPa)	524	15.99	0.0305	711	8.43	0.0119
E (GPa)	165	13.79	0.0836	164	29	0.1768
elongation %	23	5.41	0.2234	20.6	7.54	0.3656

Table 5: Properties of CFRP and epoxy adhesive based on the technical datasheet.

CFRP (ASOFABRIC-C300)		Epoxy Adhesive (ASODUR-1330)	
Thickness (mm)	0.166	Basis	two-component epoxy resin
Ultimate tensile strength (MPa)	4900	Color	amber
E (GPa)	230	Mixing ratio	3:1 (by volume, A: B)
Elongation at break (%)	2.1	Tensile strength (MPa)	55
Areal Weight (g/m ²)	300	Tensile Modulus (MPa)	1.7
		Elongation at break (%)	3
		Flexure strength (MPa)	79

Table 6: Details of the R.C. beams.

RC Beams	Damage Level up to strain in the main bars	width of CFRP (mm)	No. of Plies	Reinforcement	Average f'_c (MPa)
B1 (Control)				2- ϕ 10mm	
B2	0	150	1	2- ϕ 10mm	
B3	1800 (micro strain)	150	1	2- ϕ 10mm	43
B4	Yield	150	1	2- ϕ 10mm	
B5	3000 (micro strain)	150	1	2- ϕ 10mm	
B6	4000 (micro strain)	150	1	2- ϕ 10mm	

Table 7: Mode of failure and load and mid-span deflection at first crack, the yield of steel, and the ultimate stage.

R.C. beams	first crack		yield of steel		ultimate		Mode of Failure
	Load (kN)	δ (mm)	Load (kN)	δ (mm)	Load (kN)	δ (mm)	
B1	14.3	1.79	55.0	12.81	61.6	47.20	C.C
B2	26.8	1.36	73.9	7.85	101.0	17.73	F.D+C.C
B3			68.1	6.50	98.1	15.36	F.D+C.C
B4			80.0	7.62	102.9	17.31	F.D+C.C
B5			72.2	7.41	100.0	20.75	F.D+C.C
B6			76.9	7.17	96.0	14.27	F.D+C.C

CC: concrete crushing, F.D.: CFRP debonding

Table 8: Strain of concrete, steel, CFRP at failure.

RC beams	ϵ_c (microstrain)	ϵ_s (microstrain)	ϵ_f (microstrain)	ϵ_{fu} (microstrain)	$\epsilon_f/\epsilon_{fu}\%$
B1	-1665	3334			
B2	-----	-----	8642	21000	41.2%
B3	-1723	5342	7646	21000	36.4%
B4	-1783	2885	8025	21000	38.2%
B5	-1701	2931	8134	21000	38.7%
B6	-1553	-----	6939	21000	33.0%

ϵ_c : concrete strain, ϵ_s : steel strain, ϵ_f : CFRP strain, and ϵ_{fu} : CFRP rupture strain.

Table 9: Strength factor, stiffness, toughness, ductility factor, and performance factor.

RC beams	Strength (kN)	Strength factor (SF)	Stiffness (kN/mm)	Increase of stiffness	Toughness (kN.mm)	Ductility	Ductility factor (DF)	Performance Factor (PF)
B1	61.6	1.00	10.3	1.00	2541.6	3.7	1.00	1.00
B2	101.0	1.64	30.5	2.96	1538.9	2.26	0.61	1.00
B3	98.1	1.59	28.8	2.80	1172.6	2.37	0.64	1.02
B4	102.9	1.67	23.5	2.28	1448	2.27	0.61	1.02
B5	100.0	1.62	19.6	1.90	1811.3	2.71	0.73	1.19
B6	96.0	1.56	18.3	1.78	1325.5	2	0.54	0.84

Strength factor (S.F.): strength/ strength of the control beam.
 Ductility factor (D.F.): ductility/ ductility of the control beam.
 Performance factor (P.F.): SF X DF.

Table 10: Environmental reduction factor for various FRP systems and exposure conditions (ACI committee 440, 2004).

Exposure conditions	Fiber type	Environmental reduction factor C_E
Interior exposure	Carbon	0.95
	Glass	0.75
	Aramid	0.85
Exterior exposure (bridges, piers, and unenclosed parking garages)	Carbon	0.85
	Glass	0.65
	Aramid	0.75
Aggressive environment (chemical plants and wastewater treatment plants)	Carbon	0.85
	Glass	0.50
	Aramid	0.70

Table 11: Experimental and Analytical comparison.

R.C. beams	Experimental		ACI 440		P_{ana}/P_{exp}
	P_{exp} , (kN)	mode of failure	P_{ana} , (kN)	mode of failure	
B1	61.6	C.C	60.5	C.C	0.98
B2	101.0	F.D	110.2	F.D	1.09
B3	98.1	F.D	111.6	F.D	1.14
B4	102.9	F.D	111.8	F.D	1.09
B5	100.0	F.D	112.1	F.D	1.12
B6	96.0	F.D	114.9	F.D	1.20

Table 12: Concrete Damaged Plasticity parameters.

Dilation Angle	Eccentricity	f_b/f_{c0}	K	Viscosity Parameter
40	0.1	1.16	0.6667	0.0078

Table 13: Parameters of the Cohesive contact between CFRP and concrete substrate.

Cohesive behavior	Damage					
	Initiation		Evolution		Stabilization	
K_{nn} 1360 MPa	Normal	Tensile strength, MPa	Normal Fracture energy	0.09 mJ/mm ²	viscosity coefficient	1×10^{-5}
K_{ss} 525 MPa	Shear-1	0.7 MPa	1st shear fracture energy	0.9 mJ/mm ²		
K_{tt} 525 MPa	Shear-2	0.7 MPa	2nd shear fracture energy	0.9 mJ/mm ²		

Table 14: Experimental and FEM comparison of the R.C. beams.

R.C. beams	Experimental		FEM		Pana/Pexp	$\delta_{ana}/\delta_{exp}$
	Pexp (kN)	mid-span deflection (δ), mm	Pana, (kN)	mid-span deflection (δ), mm		
B1	61.6	31.3	63.1	29.8	1.02	0.95
B2	101.0	17.7	101.4	19.1	1.00	1.08
B3	98.1	15.4	101.6	19.3	1.04	1.26
B4	102.9	17.3	101.1	19.3	0.98	1.12
B5	100.0	20.8	100.9	19.3	1.01	0.93
B6	96.0	14.3	102.3	19.4	1.07	1.36

Figures

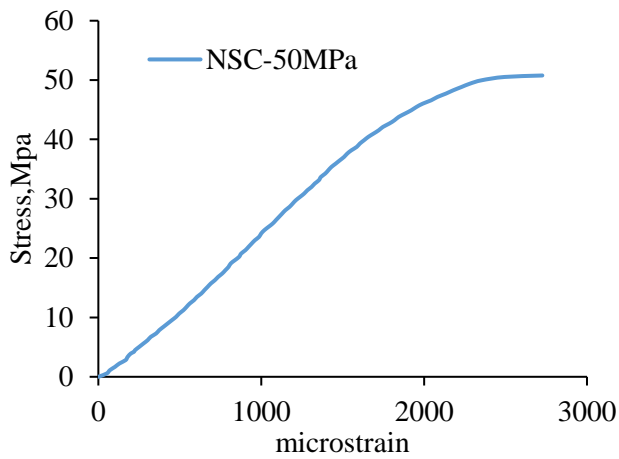


Figure 1: Stress-Strain curve of NSC using strain gauges.



Figure 2: Modulus of elasticity test using compressometer.

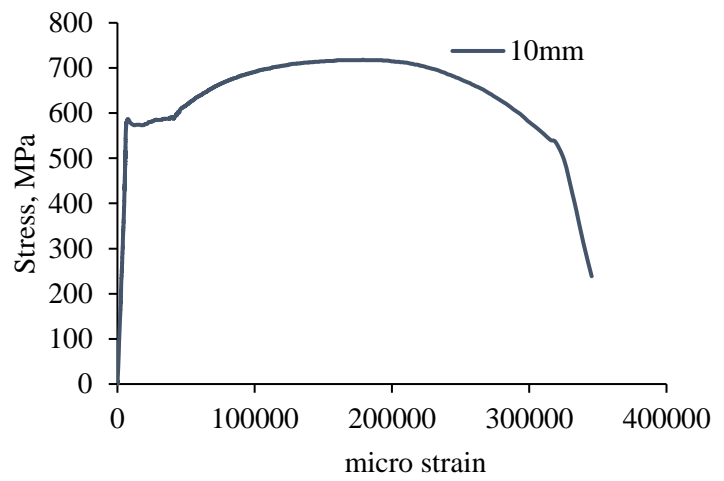
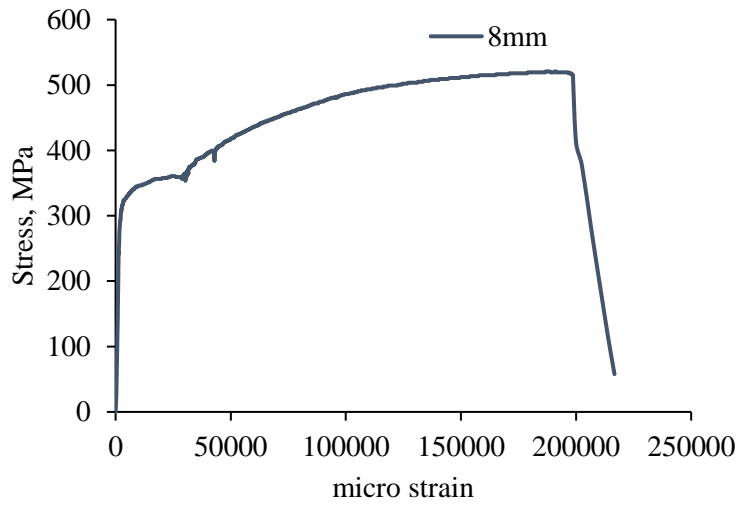
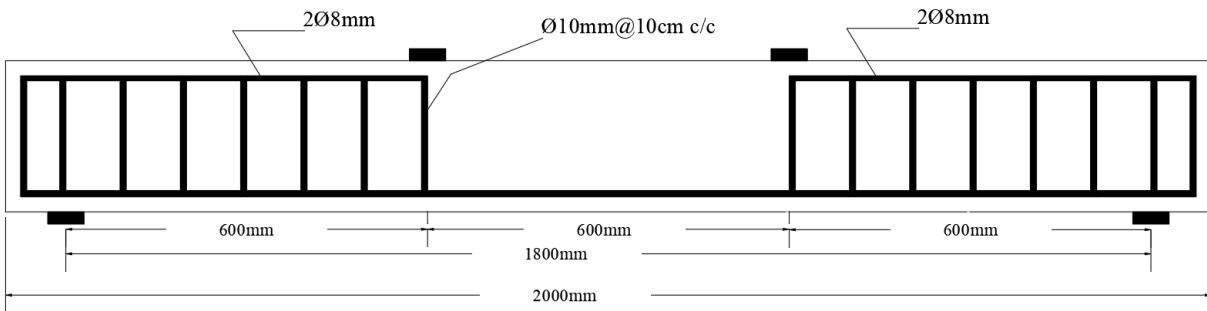


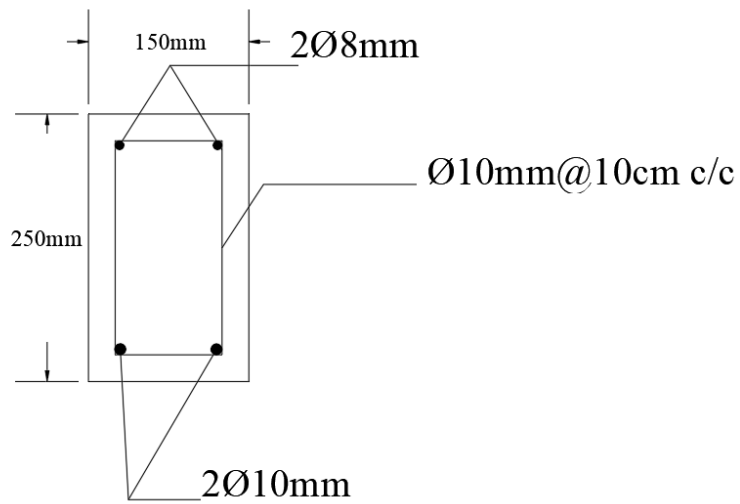
Figure 3: Tensile test of steel bars using extensometer and strain gauges and stress-strain curve for 8mm and 10mm bar.



Figure 4: CFRP and epoxy resin: (a) CFRP roller; (b) epoxy resin component A; and (c) epoxy resin component B.



Longitudinal section



Cross-Section

Figure 5: Longitudinal and cross-section of the R.C. beams.

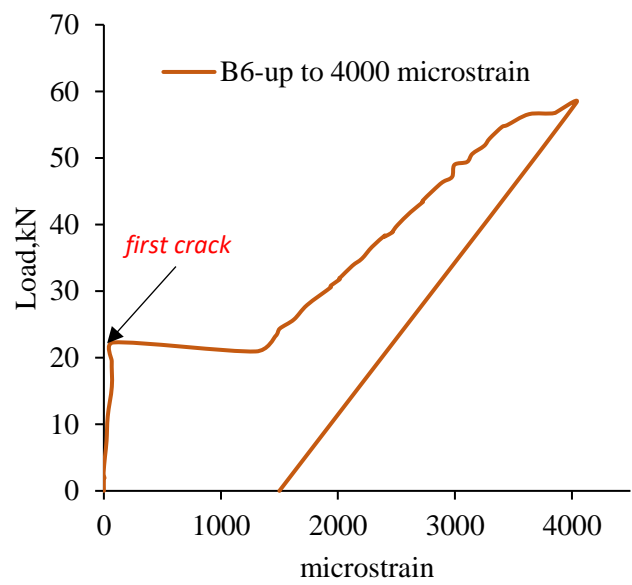
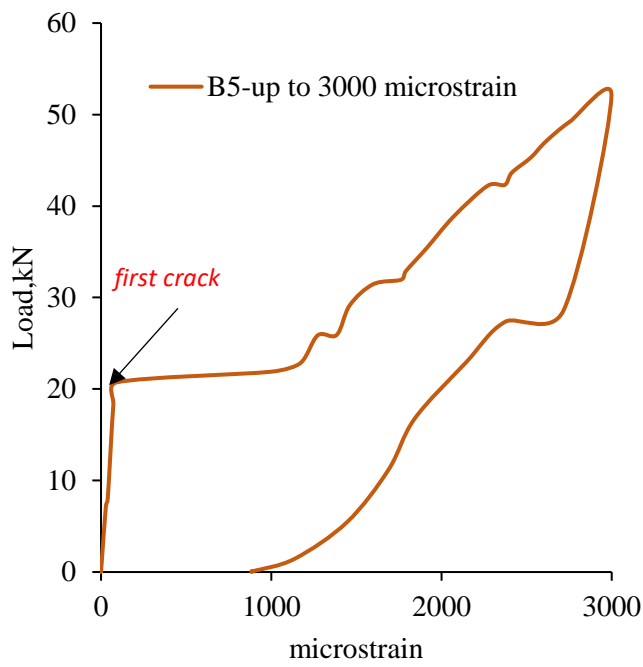
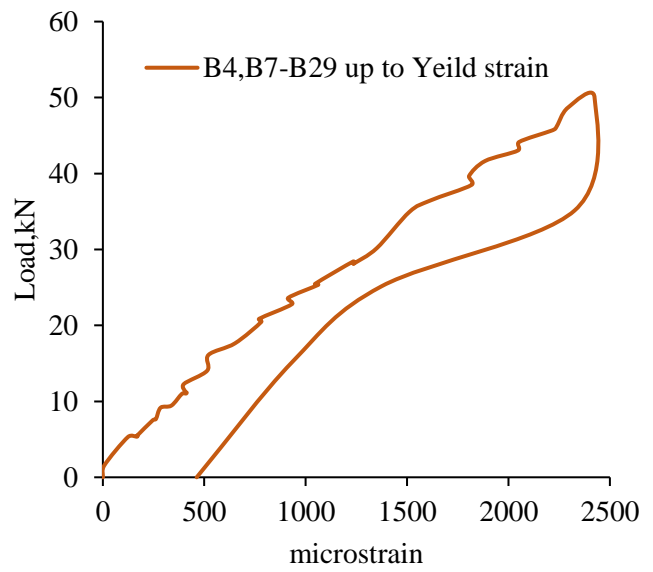
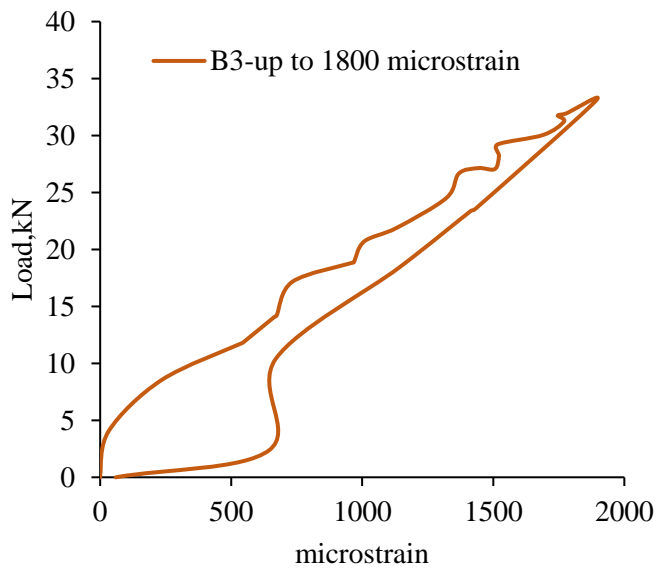


Figure 6: Load-strain relation of the damaged R.C. beams.

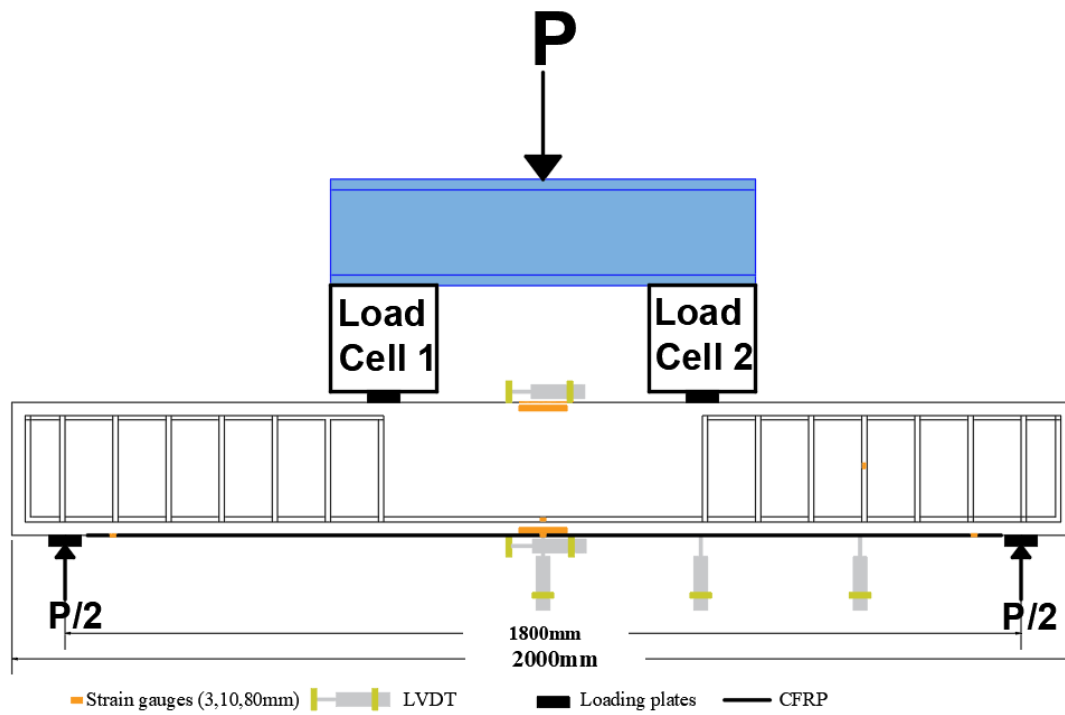


Figure 8: Loading setup and instruments.

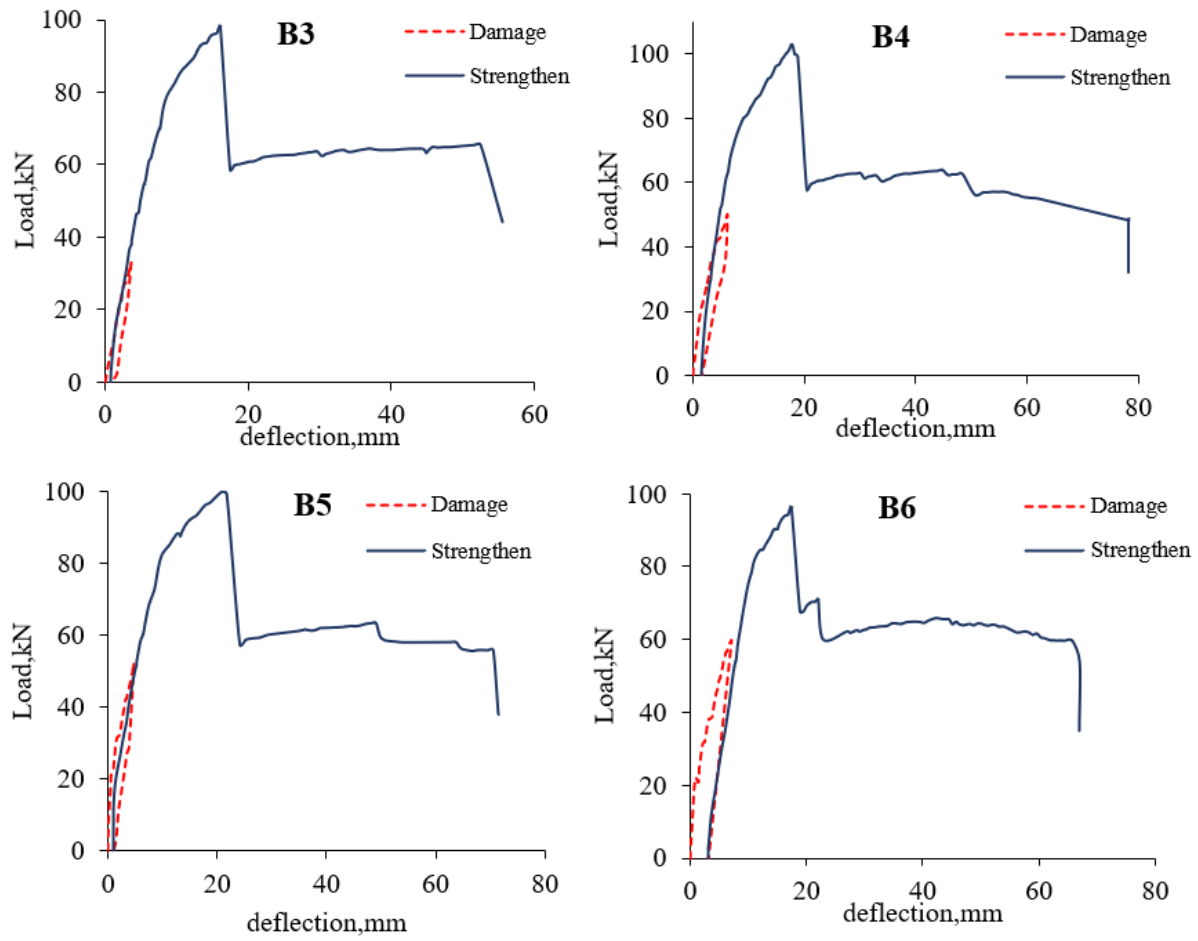


Figure 9: Load-deflection curve for pre-damage and strengthened beams.

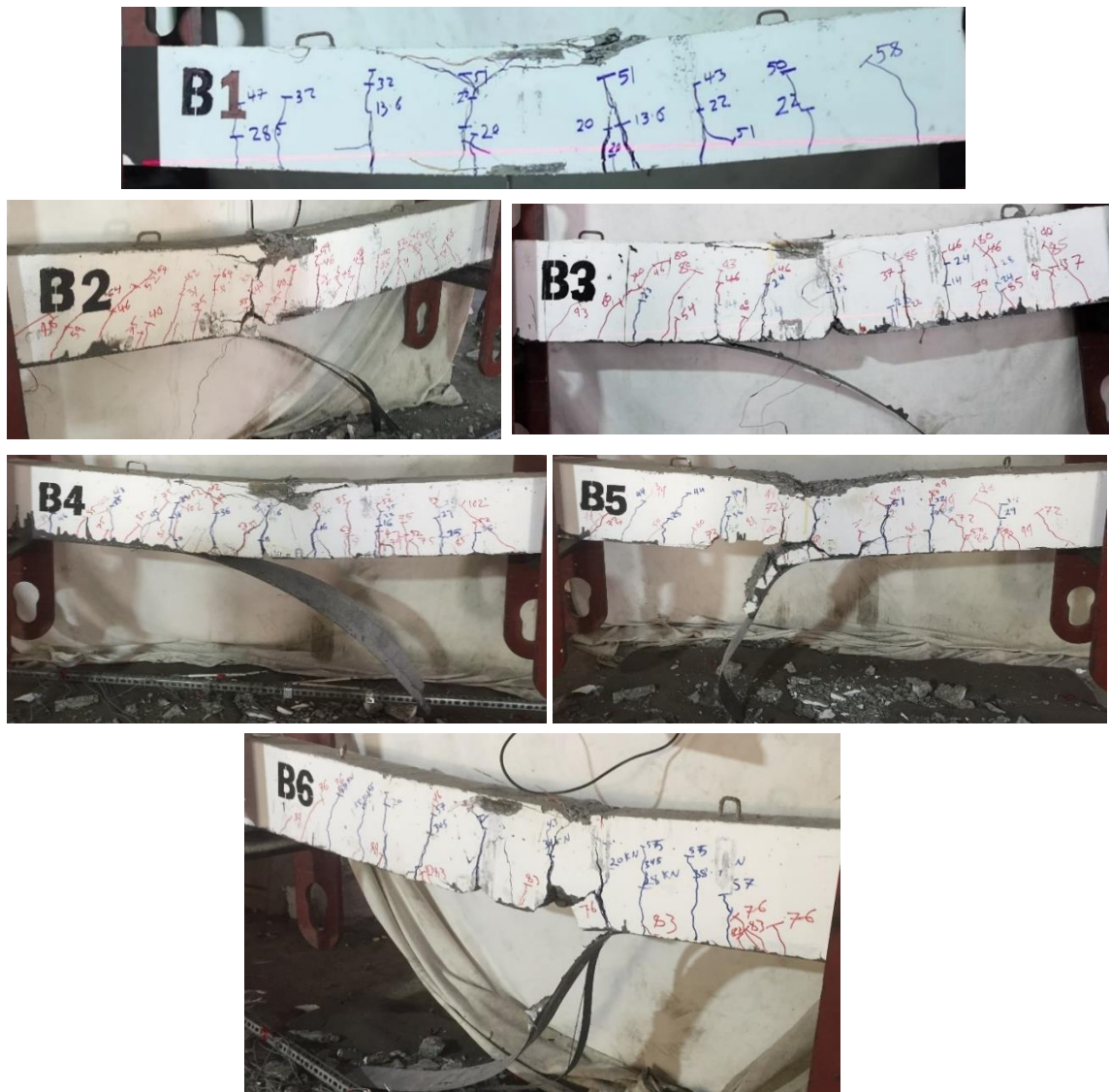


Figure 11: Failure mode of the R.C. beams: concrete crushing, B1; FRP end peeling off, B2-B4; and concrete cover separation, B5 and B6.

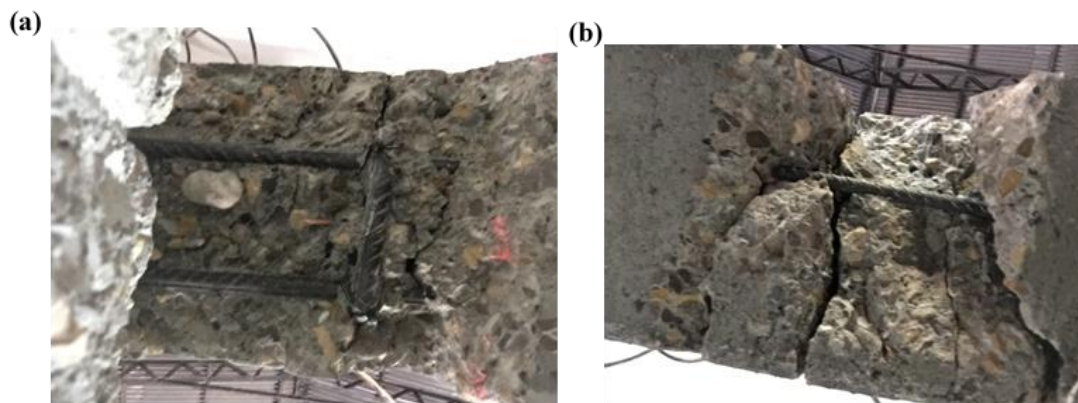


Figure 12: Cover separation bottom view; (a) B5, and (b) B6.

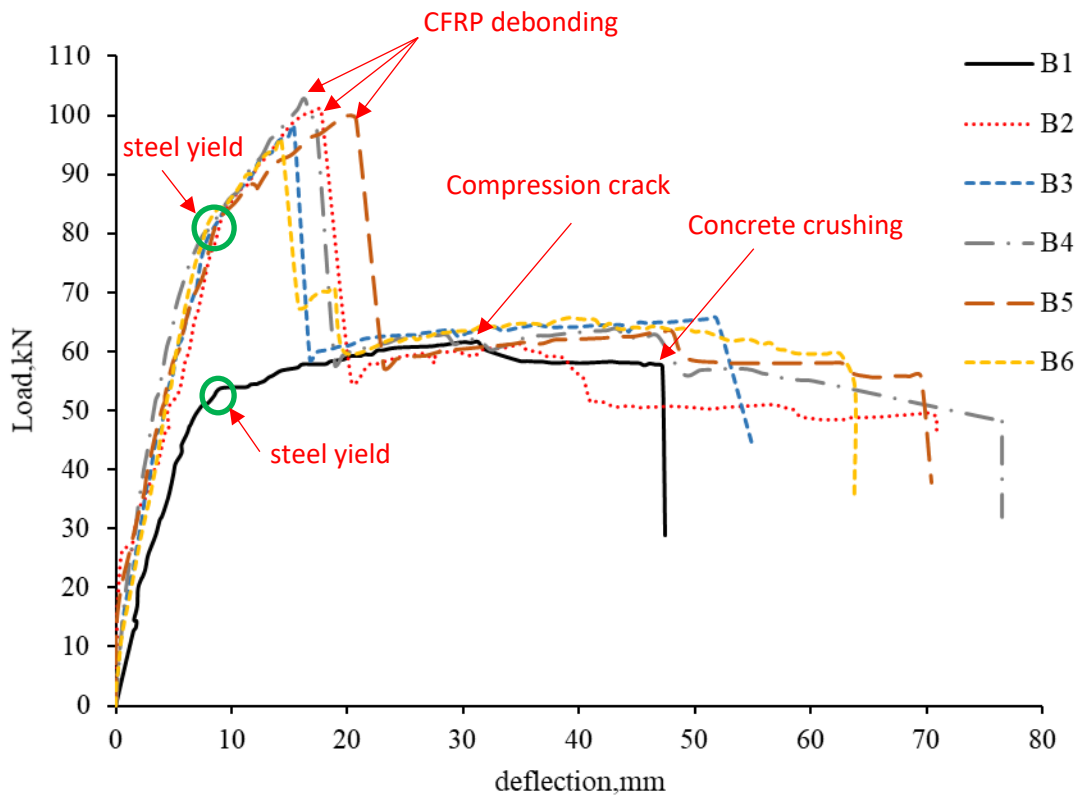


Figure 13: Load-deflection curve.

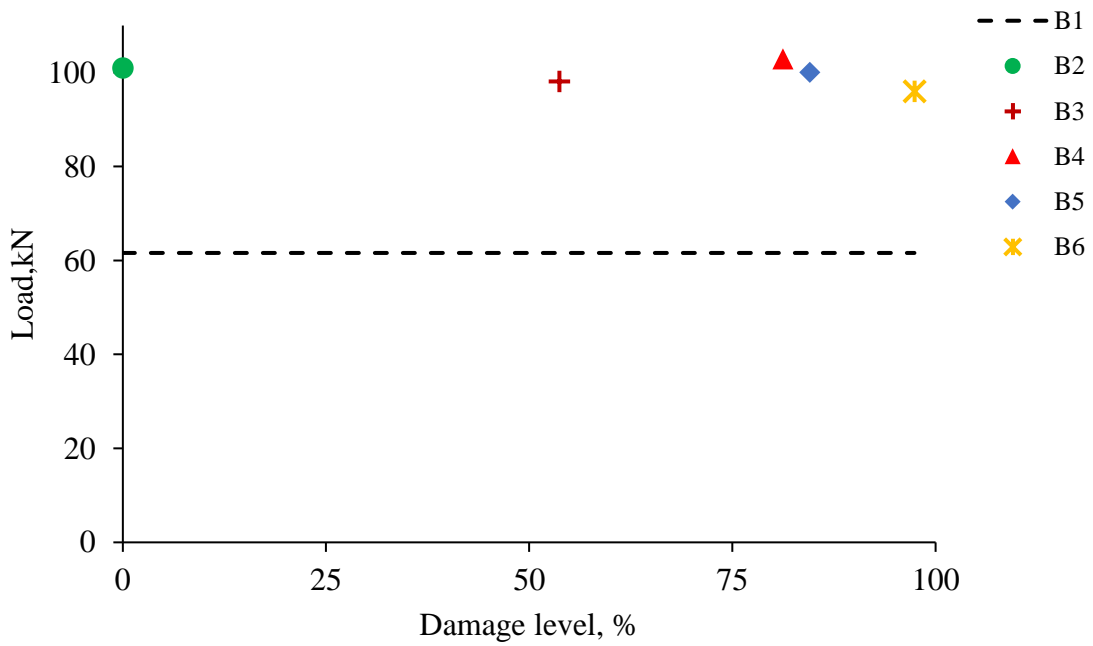


Figure 14: Ultimate load and damage levels.

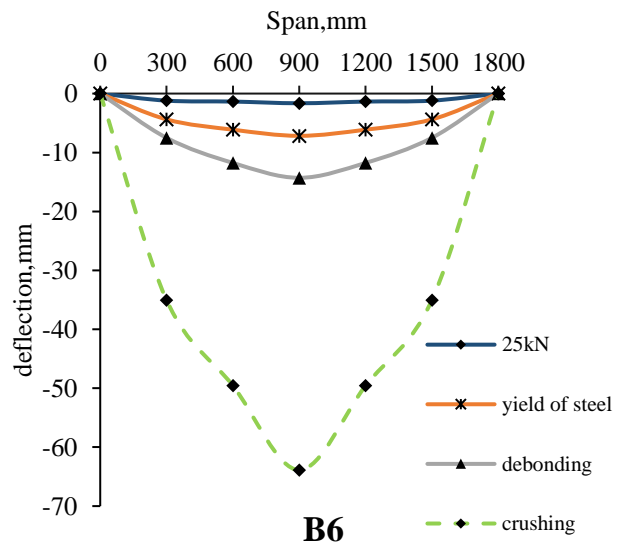
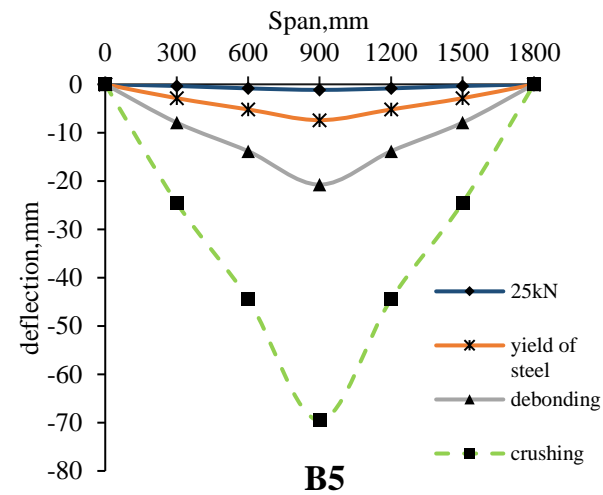
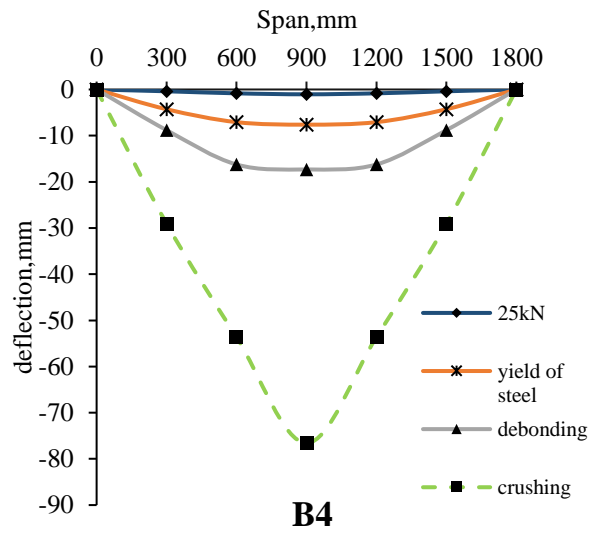
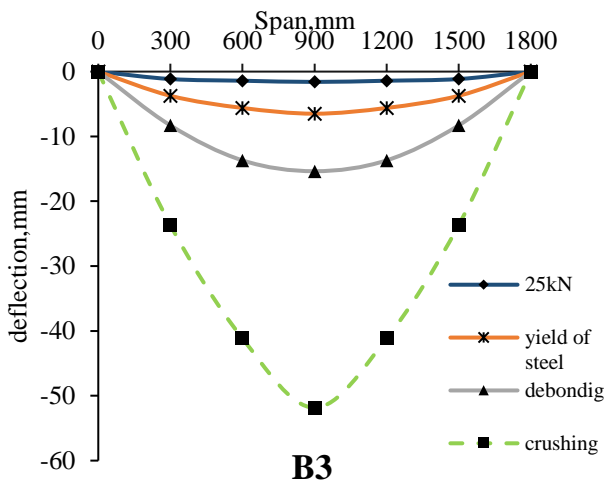
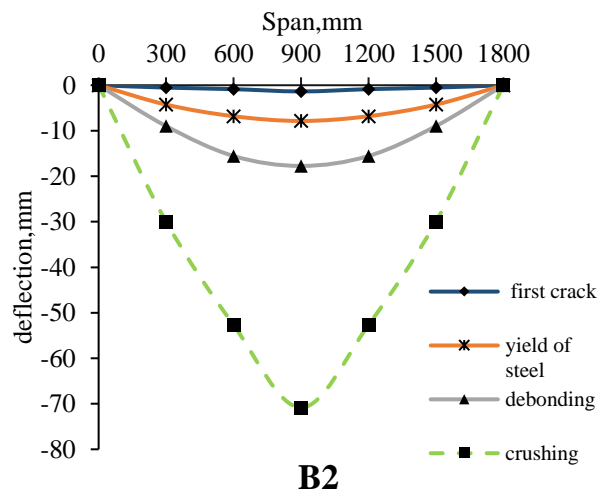
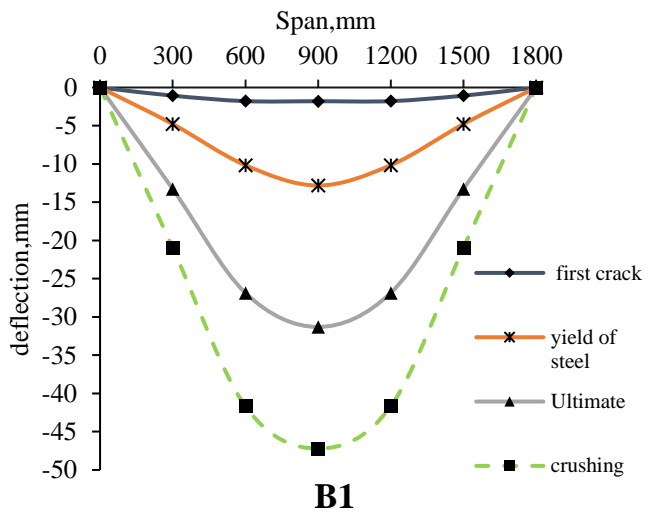


Figure 15: Deflection curve at critical loads.

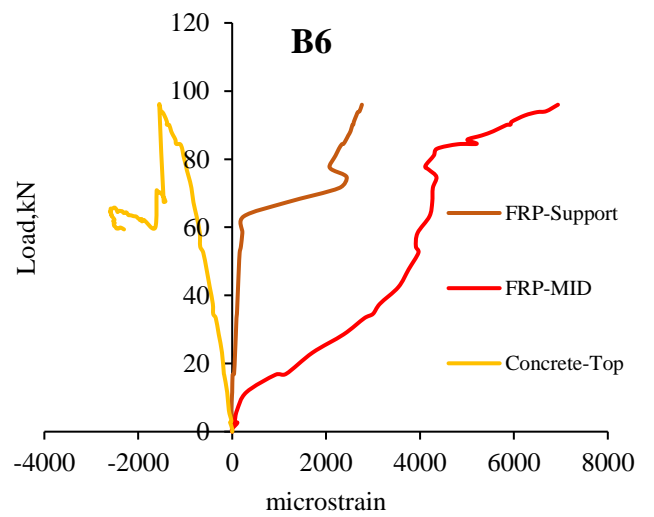
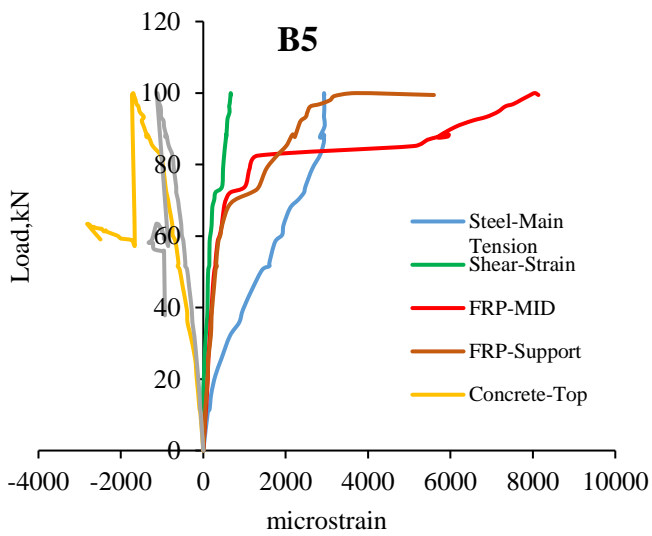
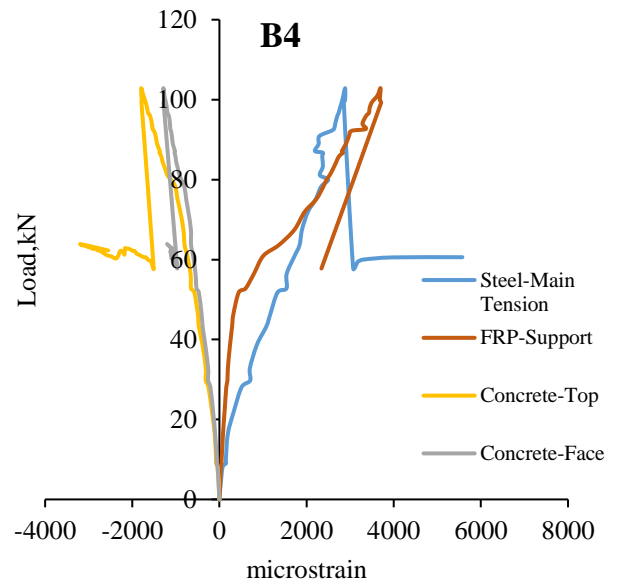
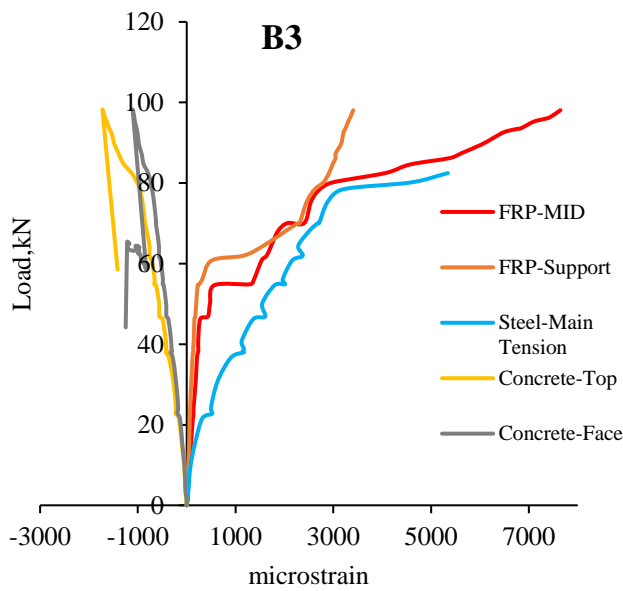
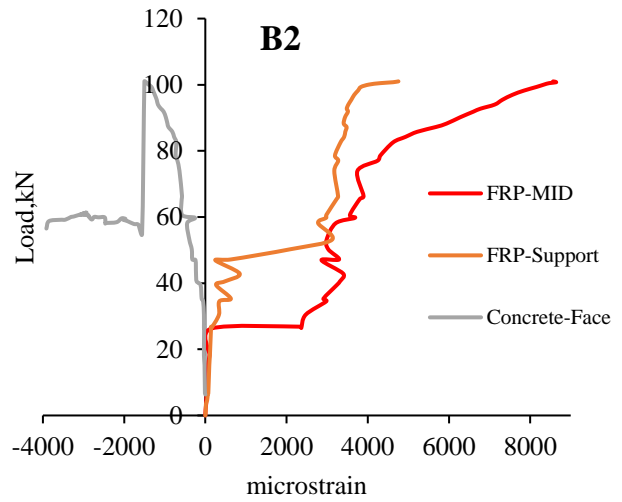
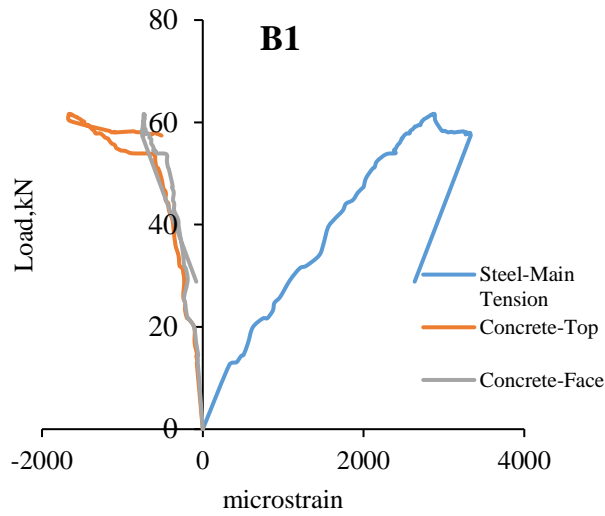


Figure 16: Load-strain curve.

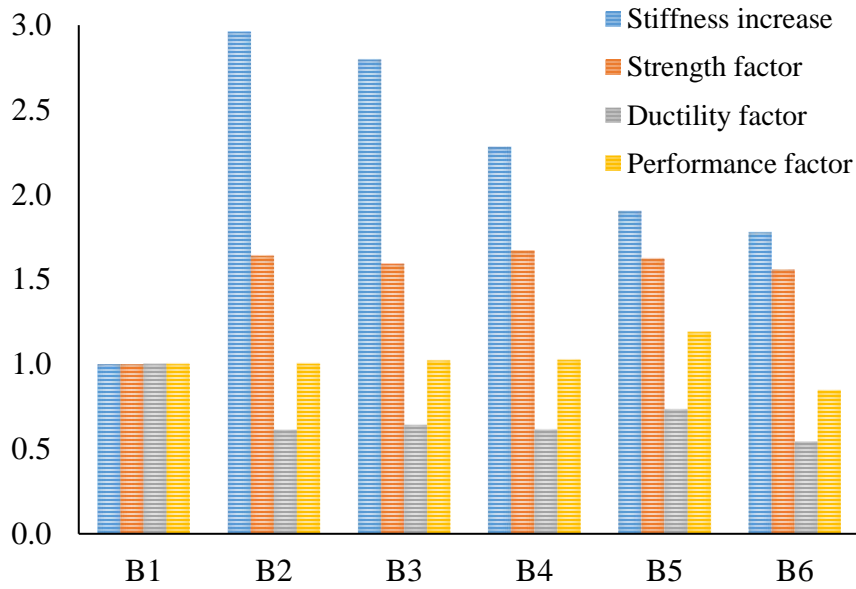


Figure 17: Stiffness increase, strength factor, ductility factor, and performance factor.

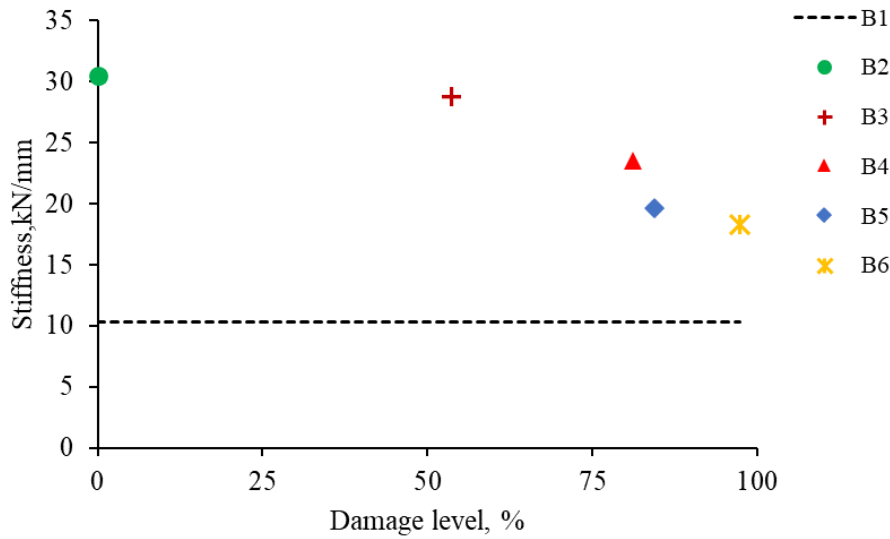


Figure 18: Stiffness and damage levels.

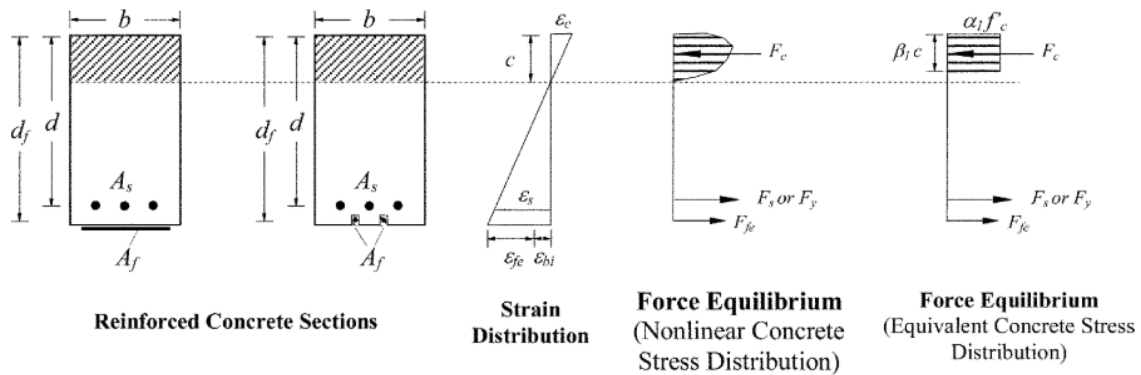


Figure 19: Internal strain and stress distribution for a rectangular section under flexure at ultimate limit state (ACI committee 440, 2004).

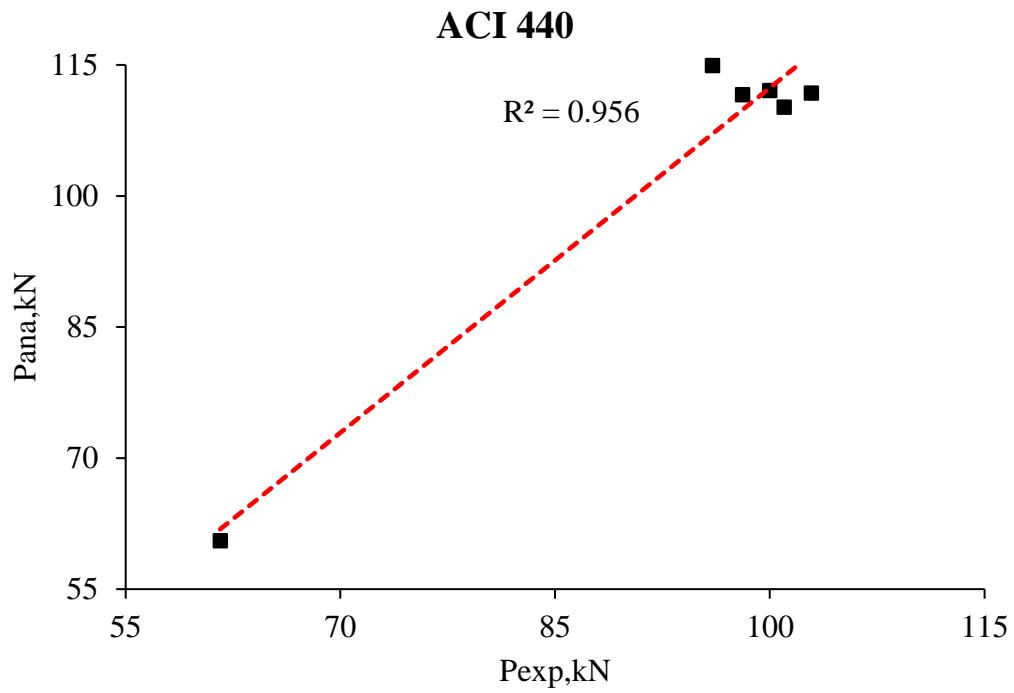


Figure 20: Relation between experimental and ACI 440 ultimate load capacity.

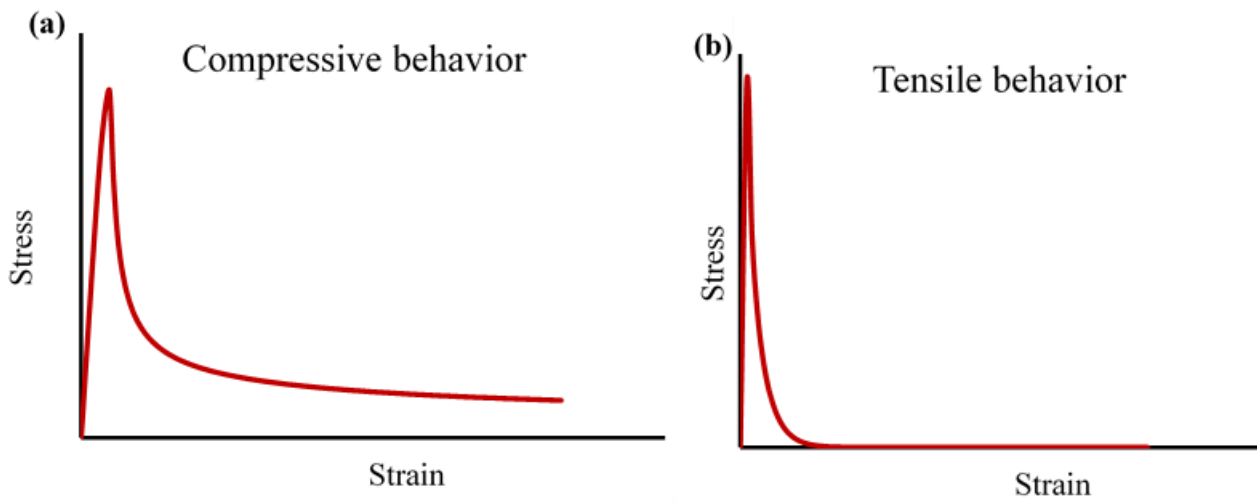


Figure 21: Concrete behavior: (a) compressive behavior, (b) tensile behavior.

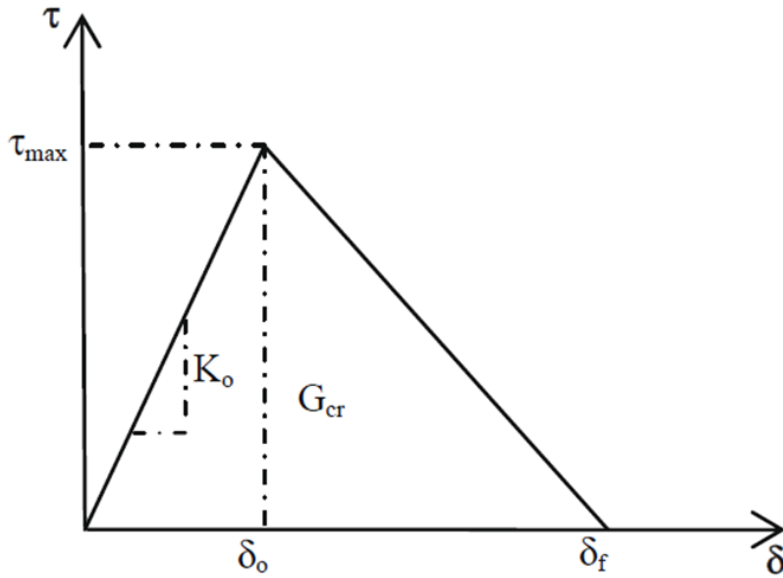


Figure 22: Bond-slip curve, bilinear model (Obaidat, 2011).

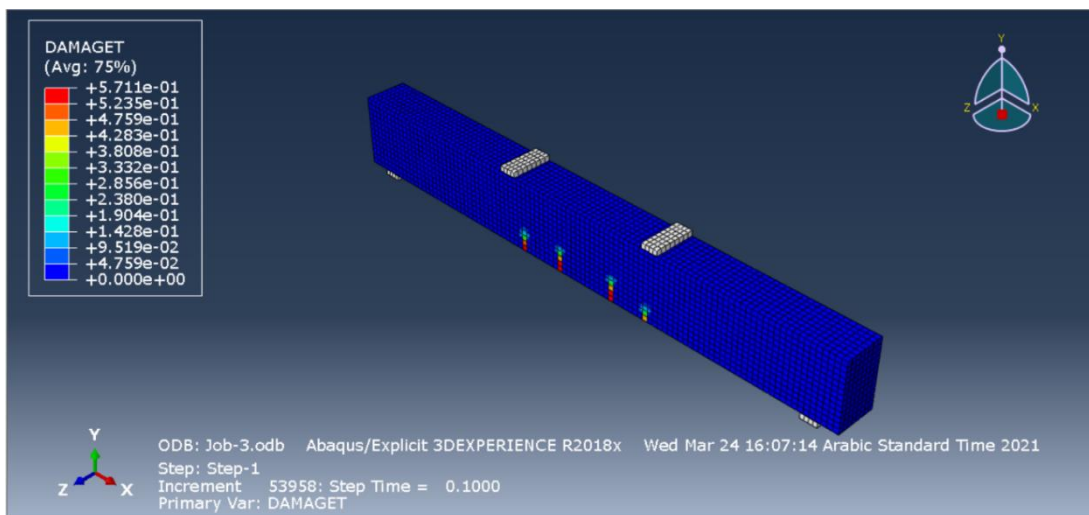


Figure 23: First crack for specimen B1.

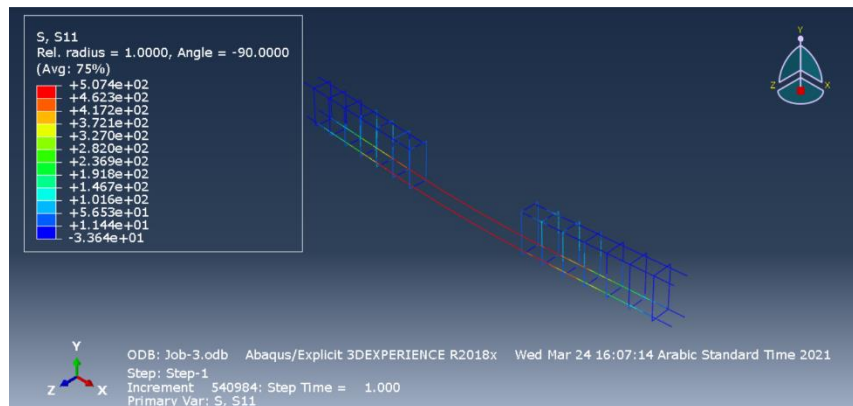


Figure 24: Stress in the reinforcement steel for the B1.

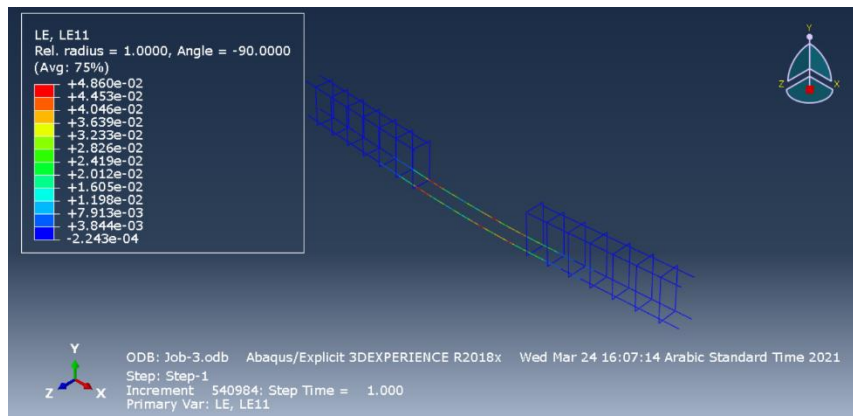


Figure 25: Strain in the reinforcement steel for the B1.

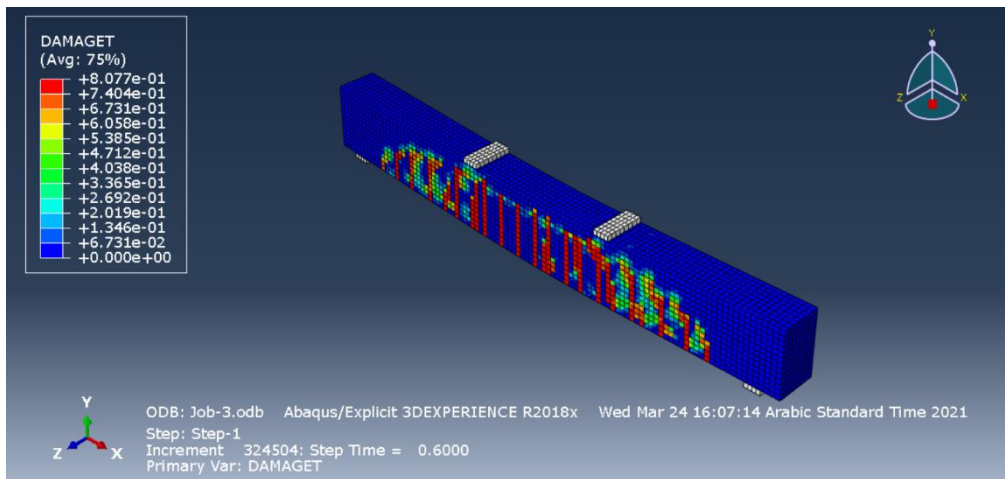


Figure 26: Crack patterns for the B1.

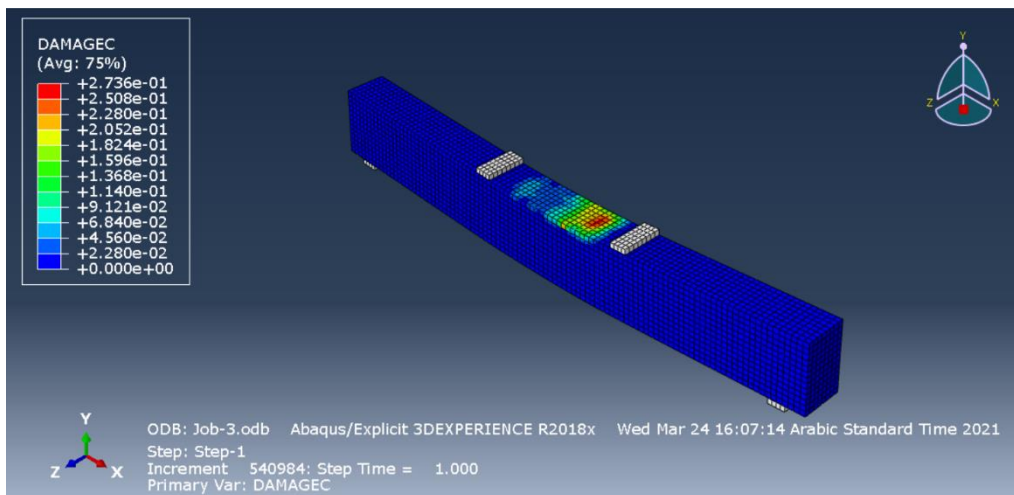


Figure 27: Concrete compression failure in the B1.

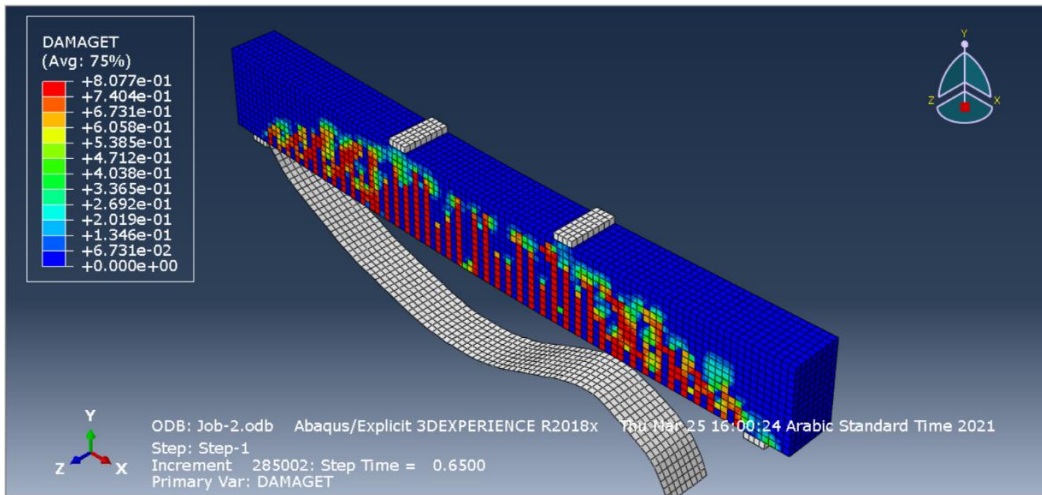


Figure 28: CFRP Debonding for the R.C. beams.

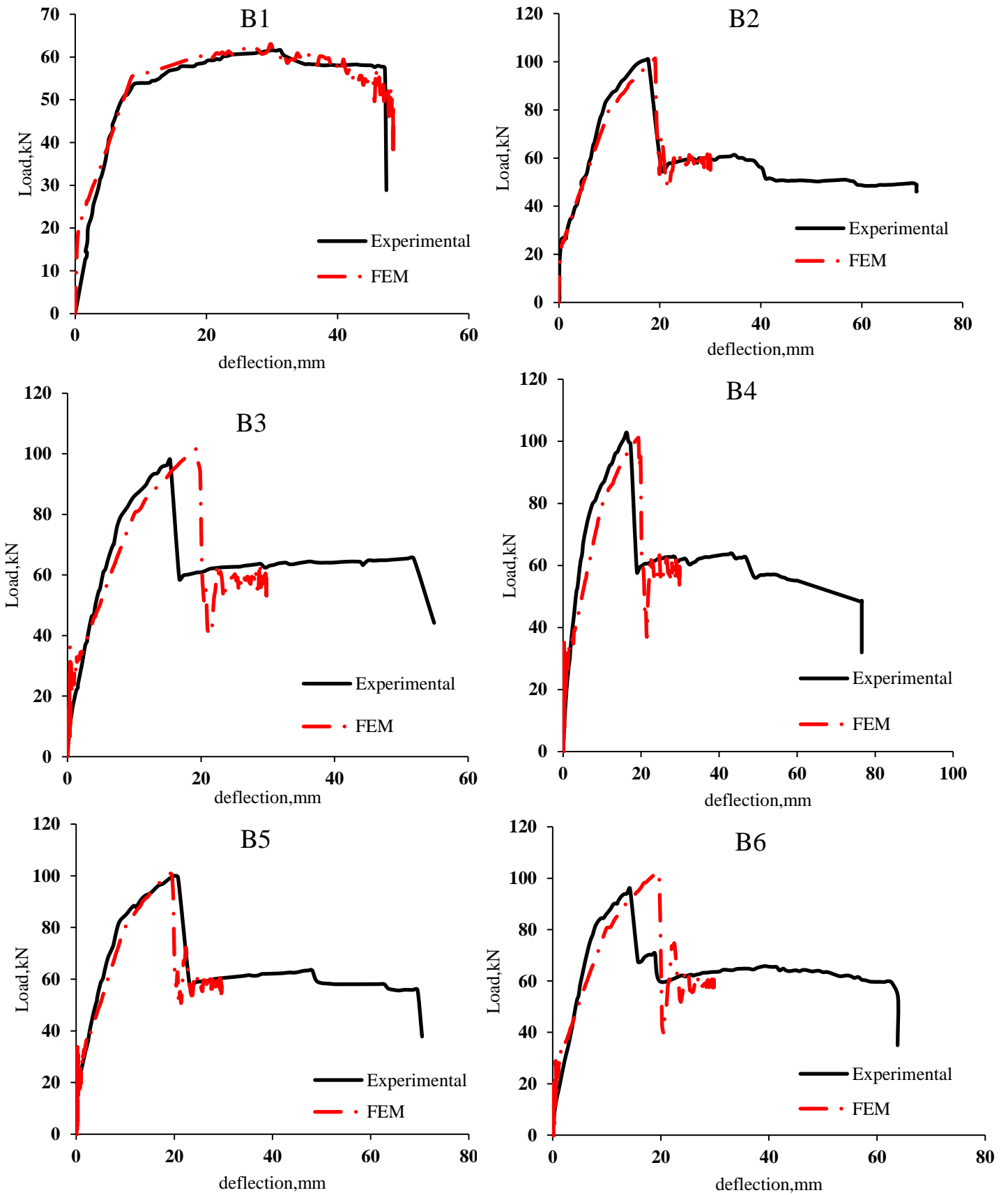


Figure 29: Experimental and F.E. Load vs. mid-span deflection for the R.C. beams.

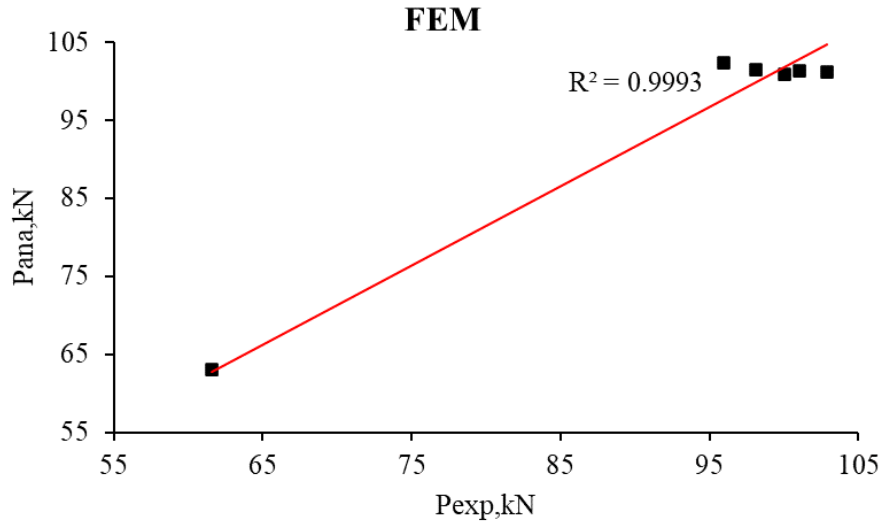


Figure 30: Relation between experimental and FEM load capacity of the R.C. beams.

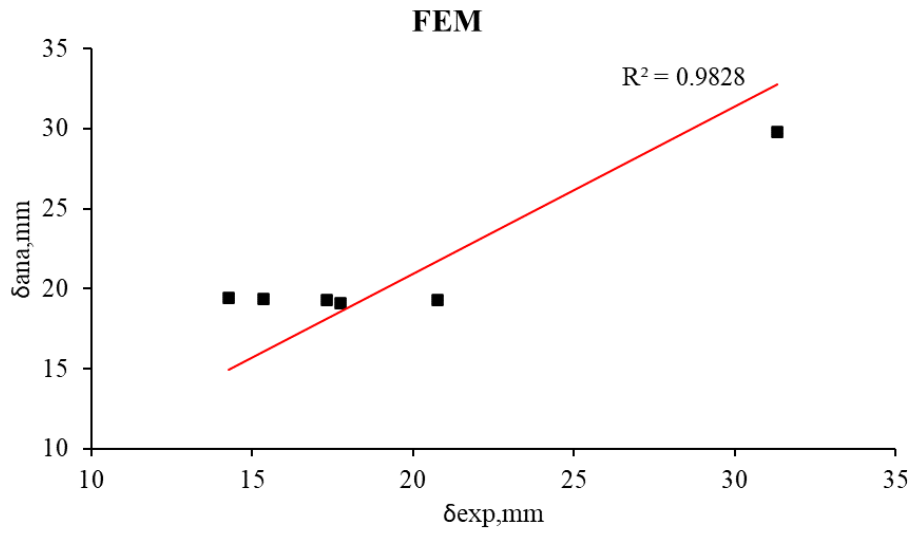


Figure 31: Relation between experimental and FEM mid-span deflection of the R.C. beams.